

**Here, in a same file, please find a point-by-point response to the reviews with a list of all relevant changes made in the manuscript, and a marked-up manuscript version.**

Interactive comment on “High occurrence of new particle formation events at the Maïdo high altitude observatory (2150 m), Reunion Island (Indian Ocean)” by Brice Foucart et al.

Manuscript published for discussion on 27 September 2017.

The authors would like to thank the reviewers for their very constructive and informative comments. These comments and suggestions have helped us to improve the quality of our manuscript, including strengthening our conclusions with additional evidences of likely precursors. Below we have responded to each of the reviewers comments. **The reviewers comments are in bold** and our responses are in normal text. You should have also received the corrected manuscript with the highlighted corrections. Please, note that several figures had been replaced by others and we added new ones.

Figures modifications:

**The Figure 2** (yearly CO variation) has is now the **b)** part of the **Figure 10**

**The Figure 3** has been modified: We added the BC dataset and is now **Figure 2**

**The Figure 4** is now **Figure 3** and composed of two figures with **a)** July 6th 2015 diurnal variation of negative ions (1-10 nm) and (10-700 nm) aerosol particle size distribution (note the different concentration scales for ion number and particle concentrations) and **b)** the BC concentration variation in  $\text{ng.m}^{-3}$

**The Figure 5** which has been changed to be **Figure 4** (DMPS spectra for 31 January and 25 March) has been displaced to the supplementary as **Figure A2**. **The Figure 4** is now “The average diurnal variation during winter and summer of the **a)** BC concentration, **(b)** number concentration of particles which diameter is larger than 100 nm ( $N_{100}$ ) and **(c)** number concentration of particles which diameter is smaller than 30 nm ( $N_{30}$ )”.

The **Figure 6** is now **Figure 5** as the **Figure 7** is 6, the 8 is 7, the 9 is 8 and the 10 is 9.

The new **Figure 9** is now composed of **a)** “The monthly  $\text{CS}_2$  and event frequency” and **b)** “The monthly  $\text{CS}_{2\text{prop}}$  exceeding the average”. The Figure 11 has been replaced by a new one.

As mentioned earlier, the new **Figure 10** is now composed of **a)** the BC concentration and **b)** the CO concentration during the year 2015

We added a new **Table 2** which deals with “The R correlation coefficients giving the relationships between NPF parameters and influencing factors”.

References modifications:

We removed several publications of the reference list which were linked to the section 2.3 removal (Potential gas-phase precursors) and added six new papers references to the text which are:

- Mirme et al., 2007 at line 157
- Kulmala et al., 2001a at line 188
- Hermann et al., 2015 at line 242
- Kiendler-Scharr et al., 2009 at line 339
- Kanawade et al., 2011 at line 339
- Freney et al., 2017 at line 339

Response to Anonymous Referee #1 comments:

Received and published on 11 November 2017,

**R1-General comment: “The work includes the experimental observation and some analytical analysis for NPF events in Reunion Island. My major comment is that several statements in this manuscript are just speculations. Without further supporting evidences, the conclusions claimed here are very shaky.”**

AR-General comment: We thank reviewer 1 for his comments on the paper and have prepared a modified version of the manuscript that take these comments into account. In this version, we deleted the section on potential gas-phase precursor sources. We have added a new analysis of boundary layer tracers that allow to partly investigate the influence of BL dynamics on the occurrence of NPF events. We have also included BC measurements that give additional hints of the potential contribution of anthropogenic precursors. We agree that this paper do not contain any precursor direct measurements of new particle precursors, but it lays as a first description of the new particle formation occurrence in this area of the world which is very poorly characterized. We now tried to avoid any speculations and we modified our conclusions.

The point-by-point response to **the detail comments** can be found below.

**RC1-1: line 69, “at low or high altitude?”**

AR1-1: We now specify high altitude line 46

**RC1-2: line 130, “Unfortunately, H<sub>2</sub>SO<sub>4</sub> was not measured” highlighted. Lines 143-144, “the major causes of SO<sub>2</sub> emissions are connected with human activities: agriculture, power plants, sugar exploitation and road traffic” highlighted, line 155, “no-direct measurements highlighted”**

AR1-2: We assume that underlining these parts is directly linked to the major comment and to which we have answered. Many papers describing NPF events at various locations do not have access to the direct measurements of NPF event precursors (which are extremely difficult to measure). Again, we hope that these measurements will take place in the future, but wish at the moment to report on the characteristics of the NPF events at the site mainly.

**RC1-3: line 169: “Format needs to be corrected”**

AR1-3: We removed the section

**RC1-4: lines 249-250: “according to Pirjola et al. (1999) Equation (2): it is not the definition of CS used in Pirjola’s article” and “the unit is not 1/s (based on the formula)”.**

AR1-4: It is true that this equation is not exactly the same than in Pirjola 1999. In fact it can be found in the following reference.

Kulmala, M., Dal Maso, M., Mäkelä, J., Pirjola, L., Väkevä, M., Aalto, P., Miiikkulainen, P., Hämeri, K., and O’Dowd, C.: On the formation, growth and composition of nucleation mode particles, *Tellus B*, 53, 479–490, 2001a.

Pirjola was the precursor of the idea that was revisited by Kulmala (2001). We now refer to Kulmala 2001a (updated in the reference list).

We believe that there is no mistake concerning the equation units.  $D_{vap}$  is in the unit of square divided by time ( $m^2 \cdot s^{-1}$ ),  $r$  is a length (nm to m conversion),  $N(r)$  is a particle number for a volume ( $part \cdot m^{-3}$ ). At the end, CS is in  $s^{-1}$ .

**RC1-5: line 256: “drained”.**

AR1-5: This a mistake and we replaced it by “dried”, as proposed line 195.

**RC1-6: lines 265-266: “Kulmala et al. (2007)” highlighted, “The GR is in the unit of hr, and the J is in the unit of second. Please unify”**

AR1-6: Growth rate were calculated in  $nm \cdot s^{-1}$  from the equation (for units homogeneity), and then reported in the text in  $nm \cdot h^{-1}$  (as specified). By convention and for clarity, we do not put units in the

equation. The Kulmala 2007 is the right reference for the exact equation that can be found in the supplement of their article.

**RC1-7: lines 265-266: “What is the unit of the number 7 list here? Based on the closure of unit here, it should be dimensionless. But why is it? And what does it stand for?”**

AR1-7: We made a typing error in that part of the equation.  $GR_{12-19}$  has to be divided by  $\Delta Dp$  which is the difference between the upper and the lower channel. Here, this is  $19 - 12 = 7$ . The equation had been corrected in the manuscript and it is now:

$$J_{12} = \frac{dN_{12-19}}{dt} + CoagS_{12} \times N_{12-19} + \frac{GR_{12-19}}{7 \text{ nm}} \times N_{12-19}$$

**RC1-8, line 272, Eq (5): “CoagS12 is in the unit of 1/s, based on the second term used in Eq (4). If so, the unit of the exponent term would be in length (eg. nm). However, this make no sense for physics.”**

AR1-8: We think again that there is no mistake concerning the equation units here.  $J_2$  and  $J_{12}$  should be in  $\text{part.m}^{-3}.\text{s}^{-1}$ . As a consequence the exponent term should be without unit. It is right because  $d_2$  is a length (m), multiplied by  $CoagS$  ( $d_2$ ) which is a time ( $\text{s}^{-1}$ ) divided by a  $GR_{12-19}$  which is a length divided by time ( $\text{m.s}^{-1}$ ).

However, we made a typing error here. We replaced the  $d_1$  in the exponent term by  $d_2$ .

$$J_2 = \frac{J_{12}}{\exp\left(-\gamma \times d_2 \times \frac{CoagS_{(d_2)}}{GR_{12-19}}\right)}$$

**RC1-9, line 276: quote missing in the Eq (7).**

Done:

$$m = \frac{\log(CoagS_{(d_{12})}) - \log(CoagS_{(d_2)})}{\log(d_{12}) - \log(d_2)}$$

**RC-1-10, line 291: “probably” highlighted, with the comment: “lots of uncertainty”.**

AR1-10: We do not have the means to evaluate if the station is in the free troposphere or not during nighttime, but we now provide indications that this is likely the case. We added to the example diurnal variation of the size distribution for a NPF the corresponding diurnal BC concentration variation (3b) in order to investigate when the NPF is taking place relative to BL advection to the site, and when BC concentrations are low, indicating FT air. We modified the end of section 4.1 as reported here (from l-228 to 254):

“The initiation of the formation of new particles at 06:00 UTC (10:00 LT) is followed by the appearance of accumulation mode particles. Further growth of the newly formed particles is generally accompanied by the simultaneous growth of the accumulation mode particles, starting around 07:00 UTC (11:00 LT), that are likely representative of the updraft of boundary layer air to the station. We computed the diurnal variation of black carbon (BC), a good indicator of any anthropogenic, hence boundary layer, influence. The corresponding diurnal variation of BC ( $\text{ng.m}^{-3}$ ) is shown on Figure 3b. BC concentration clearly increases from 06:30 UTC (when ignoring early sharp peaks that may due to local contamination), which is half an hour later than the occurrence of the cluster mode particles. Hence we can hypothesise that boundary air convection to the site is a trigger for NPF events, most particularly when the interface BL/FT is sampled. At 07:00 UTC, as the accumulation particle concentration increase from 2000 to 8000  $\text{part.cm}^{-3}$ , the BC concentration also increase to reach 630  $\text{ng.m}^{-3}$  at 09:00, when the BL is fully sampled at the site. At the end of the afternoon, the accumulation mode particles concentrations drop to less than 1000  $\text{particle.cm}^{-3}$  and BC concentrations drop to very low values. Most high altitude stations are strongly influenced by free troposphere air during nighttime regardless the season, but mostly during wintertime (Venzac et al., 2008; Rose et al., 2015a). This is also true for stations located in complex terrains such as Jungfrauoch station in the Swiss Alps (Herrmann et al., 2015) and at the Chacaltaya station in the Andes (Rose et al., 2015b). These are indicators that the station lays in the free troposphere at night. The Aitken mode particles present during nighttime at the station are hence likely present in the free troposphere and are sampled at the site in subsiding air masses (Tulet et al., 2017).

These features can also be observed on average, both for the summer and winter seasons. BC average diurnal profiles (a), together with the average diurnal variation of the number concentrations of particles larger than 100 nm ( $N_{100}$ ) (b), and the number concentration of nucleation mode particles with a diameter smaller than 30 nm ( $N_{30}$ ) (c) are shown on Figure 4. We observe that, on average, BC concentrations increase in the morning at the same time as  $N_{100}$  and  $N_{30}$ , confirming the influence of the BL on the occurrence of NPF events at the scale of the season. Moreover, we can note that during winter, BC concentrations are higher during nighttime (from 16:00 to 06:00 UTC) than during summer. This observation is also true for  $N_{100}$  with higher values from 17:00 to 02:00 UTC during winter compared to summer. We assume that during winter, trade winds favour the large scale remote primary particles transport to the Maïdo station.”

Herrmann, E., Weingartner, E., Henne, S., Vuilleumier, L., Bukowiecki, N., Steinbacher, M., Conen, F., Collaud Coen, M., Hammer, E. and Jurányi, Z.: Analysis of long-term aerosol size distribution data from Jungfrauoch with emphasis on free tropospheric conditions, cloud influence, and air mass transport, *J. Geophys. Res. Atmospheres*, 120(18), 9459–9480, 2015.

“Herrmann et al., 2015” has been added to the reference list.

Note: We replaced the 28 August 2015 Figure 3 by the 06 July 2015 one (Figure 3a) as we found that the August 28 was impacted by the volcanic plume.

**RC1-11, lines 305-306: Sentence “As shown in Figure 5. Similar seasonal trends were observed for the nucleation frequency in 2014 and 2015” highlighted with the comment: “It is not very convincing to make the conclusion of seasonal trend based on only one and half year observation.”**

AR1-11: Many studies reporting on a seasonal variation for NPF do not have more than one year and a half of data (Rodríguez et al., 2005; Suni et al., 2007; Rose et al. 2015; Berland et al., 2017; to mention only a few). We believe that one year and a half of data allows to derive a seasonal variability, especially when this seasonal variability is reproducible from one year to the other for the common months.

Berland, K., Rose, C., Pey, J., Culot, A., Freney, E., Kalivitis, N., Kouvarakis, G., Cerro, J. C., Mallet, M., Sartelet, K., Beckmann, M., Bourriane, T., Roberts, G., Marchand, N., Mihalopoulos, N. and Sellegri, K.: Spatial extent of new particle formation events over the Mediterranean Basin from multiple ground-based and airborne measurements, *Atmospheric Chem. Phys.*, 17(15), 9567–9583, doi:10.5194/acp-17-9567-2017, 2017.

Rodríguez, S., Van Dingenen, R., Putaud, J.-P., Martins-Dos Santos, S. and Roselli, D.: Nucleation and growth of new particles in the rural atmosphere of Northern Italy—relationship to air quality monitoring, *Atmos. Environ.*, 39(36), 6734–6746, doi:10.1016/j.atmosenv.2005.07.036, 2005.

Suni, T., Kulmala, M., Hirsikko, A., Bergman, T., Laakso, L., Aalto, P. P., Leuning, R., Cleugh, H., Zegelin, S. and Hughes, D.: Formation and characteristics of ions and charged aerosol particles in a native Australian Eucalypt forest, *Atmospheric Chem. Phys. Discuss.*, 7(4), 10343–10369, 2007.

Please note that we also changed the sentence at line 263: **As shown in Figure 5, similar seasonal variations were observed for the nucleation frequency in 2014 and part of 2015.**

**RC1-12, lines 311-312: “Because of a lack of knowledge about the potential gas precursor variation at Reunion Island, it is quite difficult to explain the event frequency variation with respect to the sources”** highlighted, with the comment: **“This is very critical. In this manuscript, several statements are just speculations but not conclusions. There are several missing measurements, such as gas precursors, SO<sub>2</sub> etc., hence the insight provided here is very limited.”**

AR1-12: We removed this sentence and we now reformulated this section to investigate only how physical parameters may influence the NPF frequency of occurrence and moved this part to section 4.4 where it belongs better. We also added the **Table 2** which gives more statistic details about the existing relationships between the main characteristics of the NPF events and the influencing factors. From line 327 to line 355:

**“We also computed in Table 2 the existing relationships between the monthly average meteorological parameters and the ones of the main characteristics of the NPF events.** We observe that radiation is highest between September and November (272.19 W.m<sup>-2</sup> on average), coinciding with one period of high NPF frequency (Fig. 4), but not with the maximum frequency of occurrence (March to May), nor with any high values of the GR or J<sub>2</sub>/J<sub>12</sub> (Figs. 6 and 7). **As a consequence, no correlation is observed between radiation and the NPF variables.** Hence, the availability of light for photochemistry is not the only parameter influencing the NPF frequency, **nor the formation rates or growth.** The temperature averages are higher from November to April (14.02 °C). **We find a significant (at the 95% confidence level) anti-correlation between temperature and the nucleation rate and GR.** However, the seasonal temperature variations are similar to the seasonal variation of the NPF event frequency **even if the correlation is not significant at the 95% confidence level.** Emissions of terpenes is favoured at higher temperatures **(Yu et al., 2017) while higher radiation is favouring the isoprene emissions.** Some studies have shown that high concentration of isoprene relative to monoterpene can inhibit new particle formation while favouring particle

growth (Kiendler-Scharr et al., 2009; Kanawade et al., 2011; Freney et al., 2017). This effect could partly explain that higher temperatures favour the nucleation frequency occurrence but lead to lower growth rates. Other factors such as a direct effect of temperature on the saturation vapour pressure of condensable gases can also influence this result.

The relative humidity values are typical of an inter-tropical island with peaks in summer, between December and March (76.79% on average), and the lowest values obtained in July and September. Cloudy conditions were previously shown to inhibit formation of new particles, by scavenging newly formed clusters (Venzac et al., 2007). They might also decrease photochemical processes at the origin of the formation of condensable species contributing to the growth of clusters to stable particles. At Chacaltaya, Bolivia (5200 m a.s.l), Rose et al. (2015b) reported high frequencies during the southern winter, which coincide with the dry season. For the Maïdo station, frequency variations are not fully synchronized with the dry or wet periods as defined in Fig 8b. However, there is some uncertainty both in the dry/wet season segregation and with the exact identification of maxima/minima in the seasonal variation of the NPF frequency. When considering relative humidity, we do not find any link between RH and the nucleation frequency (Table 2) but a significant anti-correlation with the formation rate: low RH values correspond to the July-August-September nucleation peak. This would be in agreement with the results from the CHC station. Figure 8b shows that the appearance time of the ultrafine particles seasonal variation is well correlated to the sunrise.

Moreover, the discussion on the potential role of different sources has been dropped but an additional section was added that discusses the common seasonal features of NPF characteristic and the ones of BC concentrations in section 4.6 (from line 396 to 407):

“Potential precursors may be of anthropogenic origin and we investigated their potential contribution by using BC as a tracer. Figure 10a and 10b show the monthly mean concentrations of BC and CO over the year 2015. The best similarity between the seasonal variations of BC and the ones of NPF parameters is found for the nucleation rate (Table 2). This may indicate that air masses influenced by a larger contribution of anthropogenic compounds are favourable to more intense NPF events, but not necessarily more frequent. Indeed, moderately high NPF frequencies are observed for high BC monthly mean values during the spring period, but the high frequencies of NPF event occurrence observed during the autumn period are not associated to very large BC monthly mean concentrations, and thus other contributors are expected during autumn. The growth rate of newly formed particles is best correlated to CO concentrations (Table 2). This suggests that CO and BC do not have the exact same sources. CO may originate from other sources than combustion process, such as marine source. This result also confirms that condensable species necessary to form new particles are hence likely different from the ones responsible for their further growth.”

**RC1-13, lines 341-343:** “on average, the GRs were enhanced during the wet period, which is not in agreement with the present study, as we find high medians during the dry period (22.82 nm.h<sup>-1</sup> averaged from July to November)” highlighted with the comment “Any explanation or comment for this?”

AR1-13: Several reasons may explain these discrepancies, such as the topography of each station relative to cloud location during the wet season, or the seasonal variation of condensable species responsible for the particle growth. We now added this in the text. However, we do not have enough information on the respective factors that may induce such a discrepancy and we could only introduce more speculation that we want to avoid.

**RC1-14, lines 360-362: “The peak in July is correlated to the Somalian phytoplankton bloom, which indicates a possible influence of a marine source on the NPF intensity during this month”** highlighted

AR1-14: Yes, we agree that this is speculation, and do not mention this coincidence anymore in the discussion and the conclusion.

**RC1-15: “arbitrarily” is highlighted, with the comment: “Why arbitrarily? Will selecting different values result in different conclusion? Need justification of this threshold value“.**

AR1-15: The value chosen is not totally arbitrary. We started our investigation by choosing the median CS over the whole year as a threshold value. We then increase and decreased this threshold so we have a reasonable seasonal variation of days exceeding this threshold values. Choosing other threshold values would have led to less pronounced seasonal variability, but would not have changed the shape of the seasonal variability. We added new sentences at lines 385 - 389:

“We started our investigation by choosing the median CS over the whole year as a threshold value. We then used an iteration process to fix the threshold so we have a reasonable seasonal variation of days exceeding this threshold values. Choosing other threshold values within CS<sub>2ev</sub> and CS<sub>2noev</sub> medians range would have led to less pronounced variability but would not have changed the shape of the seasonal trend”.

**RC1-16, line 441: “modelling methods” highlighted, with the comment: “What kind of modelling methods mentioned here? “**

AR-16: It would be helpful to perform back-trajectories analysis (of the flexpart type) with a fine resolution to take into account the local and complex atmospheric dynamic at the Maïdo observatory. We could also use mesoscale atmospheric models such as Meso-NH, but this would need to include all potential sources of precursor gases and a good nucleation parameterisation. We now mention the models that would be useful in the text at lines 424 – 429:

“At Reunion Island, the identification of different sources contributing to the gas phase composition of the atmosphere is not well established. To complete this work, it would be valuable to have direct measures of the cluster ion composition that would provide indication of the anthropogenic, vegetation or marine sources contributions to nucleation at the site. In addition and although they are complex, modelling methods such as a

detailed back-trajectory analysis should be used to understand the origin of the local air masses and source contributions at the Maïdo observatory.”

Response to Anonymous Referee #2 comments:

Received and published: 10 November 2017,

We thank also reviewer 2 for his constructive remarks and suggestions of improvement that were all taken into account:

**RC2-1: Does the elimination of 47 days that occurred during the three eruptive periods, along 61 days of missing data, have an impact on your results pertaining to seasonality of NPF. From Figure 5, it appears that a significant number of days in 2015 were not considered during the winter (Feb and March), and there was not overlap with 2014 data for confidence. My concern arises due to the statistics of small numbers considered. Often the months with lower NPF frequency (near or below the annual average) are represented by the months with a more complete dataset (30-31 days). Would you provide more information or statistics showing that you are representing each season with a similar amount of data?**

AR2-1: On figure 4, the numbers of days which were taken into account for the occurrence calculation are indicated on the top of the figure. For the high frequency period of autumn 2015 (March-April), March has a low fraction of days available for analysis (14), while April has a high fraction of days available for analysis (30) with both indicating a high NPF occurrence frequency. Throughout the June to September period, there is a very consistent increase of NPF frequency of occurrence, whatever the year considered and whatever the number of days available (ranging from 11 to 30). This, in our opinion, would indicate that even the months with a low number days available for the NPF frequency of occurrence are reliable.

**RC2-2: This is especially relevant since you are contrasting your results with those reported by Rose et al. (2015), and do not see NPF governed by dry/wet seasons. The paper continues with potential explanation for these differences.**

AR2-2: Thanks for this remark. We actually moderated our argumentation on the contrast with the results from Rose et al. taking into account the uncertainty on the frequency seasonal variability. We now argue in section 4.4 (from line 344 to 354):

“Cloudy conditions were previously shown to inhibit formation of new particles, by scavenging newly formed clusters (Venzac et al., 2007). They might also decrease photochemical processes at the origin of the formation of condensable species contributing to the growth of clusters to stable particles. At Chacaltaya, Bolivia (5200 m a.s.l), Rose et al. (2015b) reported high frequencies during the southern winter, which coincide with the dry season. For

the Maïdo station, frequency variations are not fully synchronized with the dry or wet periods as defined in Fig 8b. However, there is some uncertainty both in the dry/wet season segregation and with the exact identification of maxima/minima in the seasonal variation of the NPF frequency. When considering relative humidity, we do not find any link between RH and the nucleation frequency (Table 2) but a significant anti-correlation with the formation rate: low RH values correspond to the July-August-September nucleation peak. This would be in agreement with the results from the CHC station.”

**RC2-3: This becomes more evident in Section 4.4. The meteorological variables are discussed in reference to the monthly NPF frequency, monthly averaged GR and monthly averaged formation rates. I would encourage the authors to instead consider robust statistical methods to look for significance (or lack thereof) between these meteorological variables (along with CO) and NPF frequency, GR or formation rates. For example, do you see correlation on the daily level between NPF frequency and threshold values of gas concentration or state variables? This section is inconclusive.**

AR2-3: This is a good suggestion and we added a new Table 2 showing the statistical analysis of the relationships between NPF parameters (occurrence, GR and Js) and influencing factors (Ray, RH, T, P, CS<sub>2</sub>, CS<sub>2prop</sub>, CO and BC). Correlations have been calculated from the monthly averages of each parameters. Taking a degrees-of-freedom value of 10 and a risk  $\alpha = 0.05$  (95% of confidence), we obtained a lower limit value of 0.576. Table 2 usually quantitatively confirms the observed co-variations that were pointed out previously in this section and we believe there we are now more conclusive (from line 326 to 342):

“We also computed in Table 2 the existing relationships between the monthly average meteorological parameters and the ones of the main characteristics of the NPF events. We observe that radiation is highest between September and November (272.19 W.m<sup>-2</sup> on average), coinciding with one period of high NPF frequency (Fig. 4), but not with the maximum frequency of occurrence (March to May), nor with any high values of the GR or J<sub>2</sub>/J<sub>12</sub> (Figs. 6 and 7). As a consequence, no correlation is observed between radiation and the NPF variables. Hence, the availability of light for photochemistry is not the only parameter influencing the NPF frequency, nor the formation rates or growth. The temperature averages are higher from November to April (14.02 °C). We find a significant (at the 95% confidence level) anti-correlation between temperature and the nucleation rate and GR. However, the seasonal temperature variations are similar to the seasonal variation of the NPF event frequency even if the correlation is not significant at the 95% confidence level. Emissions of terpenes is favoured at higher temperatures (Yu et al., 2017) while higher radiation is favouring the isoprene emissions. Some studies have shown that high concentration of isoprene relative to monoterpene can inhibit new particle formation while favouring particle growth (Kieindler-Scharr et al., 2009; Kanawade et al., 2011; Freney et al., 2017). This effect could partly explain that higher temperatures favour the nucleation frequency occurrence but lead to lower growth rates. Other factors such as a direct effect of temperature on the saturation vapour pressure of condensable gases can also influence this result.”

We also use it in section 4.5 (condensation sink) from line 392 to 394:

“Hence, we actually find a similar seasonal variation between the frequency of CS exceeding a threshold value and the frequency of occurrence of NPF events (also shown by Table 2). This strengthens the hypothesis that there are precursors potentially transported simultaneous to aerosols from lower altitudes.”

And in the new section 4.6 (black carbon, the anthropogenic distribution) from line 396 to 407:

“Potential precursors may be of anthropogenic origin and we investigated their potential contribution by using BC as a tracer. Figure 10a and 10b show the monthly mean concentrations of BC and CO over the year 2015. The best similarity between the seasonal variations of BC and the ones of NPF parameters is found for the nucleation rate (Table 2). This may indicate that air masses influenced by a larger contribution of anthropogenic compounds are favourable to more intense NPF events, but not necessarily more frequent. Indeed, moderately high NPF frequencies are observed for high BC monthly mean values during the spring period, but the high frequencies of NPF event occurrence observed during the autumn period are not associated to very large BC monthly mean concentrations, and thus other contributors are expected during autumn. The growth rate of newly formed particles is best correlated to CO concentrations (Table 2). This suggests that CO and BC do not have the exact same sources. CO may originate from other sources than combustion process, such as marine source. This result also confirms that condensable species necessary to form new particles are hence likely different from the ones responsible for their further growth.”

**RC2-4: Section 4.5 is very interesting, and as the authors note in contrast to previous studies, as low CS is normally associated with NPF or at least you do not expect an anticorrelation. This brings us to the conclusion that you have a precursor potentially emitted simultaneous to aerosols that are increasing CS. This is consistent with your Figure 4 (and previous reviewer’s comments pertaining to advection).**

AR2-4: Yes, we took into account this comment and reviewer’s 1 comment and now include new figure 3b showing the BC concentration diurnal variation for July 6<sup>th</sup> and new figure 4 with BC concentration mean diurnal variation,  $N > 100$  nm (accumulation mode) and  $N < 30$  nm (nucleation mode) particle concentrations for different seasons in section 4.1 with the corresponding text (from 228 to 254):

“The initiation of the formation of new particles at 06:00 UTC (10:00 LT) is followed by the appearance of accumulation mode particles. Further growth of the newly formed particles is generally accompanied by the simultaneous growth of the accumulation mode particles, starting around 07:00 UTC (11:00 LT), that are likely representative of the updraft of boundary layer air to the station. We computed the diurnal variation of black carbon (BC), a good indicator of any anthropogenic, hence boundary layer, influence. The corresponding diurnal variation of BC ( $\text{ng}\cdot\text{m}^{-3}$ ) is shown on Figure 3b. BC concentration clearly increases from 06:30 UTC (when ignoring early sharp peaks that may be due to local contamination), which is half an hour later than the occurrence of the cluster mode particles. Hence we can hypothesise that boundary air convection to the site is a trigger for NPF events, most particularly when the interface BL/FT is sampled. At 07:00 UTC, as the accumulation particle concentration increases from 2000 to 8000  $\text{part}\cdot\text{cm}^{-3}$ , the BC concentration also increases to reach 630  $\text{ng}\cdot\text{m}^{-3}$  at 09:00, when the BL is fully sampled at the site. At the end of the afternoon, the accumulation mode particles concentrations drop to less than 1000  $\text{part}\cdot\text{cm}^{-3}$  and BC concentrations drop to very low values. Most high altitude stations are

strongly influenced by free troposphere air during nighttime regardless the season, but mostly during wintertime (Venzac et al., 2008; Rose et al., 2015a). This is also true for stations located in complex terrains such as Jungfraujoch station in the Swiss Alps (Herrmann et al., 2015) and at the Chacaltaya station in the Andes (Rose et al., 2015b). These are indicators that the station lays in the free troposphere at night. The Aitken mode particles present during nighttime at the station are hence likely present in the free troposphere and are sampled at the site in subsiding air masses (Tulet et al., 2017).

These features can also be observed on average, both for the summer and winter seasons. BC average diurnal profiles (a), together with the average diurnal variation of the number concentrations of particles larger than 100 nm ( $N_{100}$ ) (b), and the number concentration of nucleation mode particles with a diameter smaller than 30 nm ( $N_{30}$ ) (c) are shown on Figure 4. We observe that, on average, BC concentrations increase in the morning at the same time as  $N_{100}$  and  $N_{30}$ , confirming the influence of the BL on the occurrence of NPF events at the scale of the season. Moreover, we can note that during winter, BC concentrations are higher during nighttime (from 16:00 to 06:00 UTC) than during summer. This observation is also true for  $N_{100}$  with higher values from 17:00 to 02:00 UTC during winter compared to summer. We assume that during winter, trade winds favour the large scale remote primary particles transport to the Maïdo station”

**RC2-5: Why was Figure 4 selected as the example plot? Does the appearance of accumulation mode particles simultaneous to the formation of new particles always happen? This was mentioned in reference to this case, but it is not clear if this happens frequently (during every season) at the site. If so, is this source of accumulation mode particles associated with a specific wind direction? This is stated in the conclusion, but this reader would appreciate more information pertaining to the details of this source**

AR2-5: As mentioned in the previous comment, we now provide a diurnal variation of BC for each season, but also show the diurnal variation of the nucleation mode ( $N_{30}$ ) and accumulation ( $N_{100}$ ) number concentration of particles for the particular case of the case study, but also for the seasonal averages.

Minor comments:

**RC2-6 line 21: term “off-season” is unclear to this reader.**

AR2-6: We agree that this term is misused and changed it to “transition periods” and specify them line 22.

**RC2-7: line 306: The statement “similar seasonal trends were observed for nucleation frequency in 2014 and 2015”, is only observed from May – Dec”.**

AR2-7: We modified this part, which is now: “As shown in Figure 5, similar seasonal variations were observed for the nucleation frequency in 2014 and part of 2015.” at line 263.

**RC2-8: line 331: typing error on “FNP”**

AR2-8: It is corrected at line 284

**RC2-9: Then, you ask a question about the GR<sub>12-19</sub> which is “Why did you choose to calculate the growth rate over such a small size range (12-19) and few bins? “**

AR2-9: The lower limit is defined by the smallest channel that we had on DMPS and the AIS data set was too reduced. The upper limit is close to those which are traditionally used in the literature.

We added a new sentence at line 199: “As the DMPS offers a much more extended data set than the AIS, we applied the method to the DMPS 12-19 nm size range for which the lower limit (12) was defined by the smallest channel of the device”

Response to the public short comment (SC1):

Received and published on 17 October 2017,

**SC1-1: Interesting paper about the occurrence and diurnal patterns of ultrafine particles at a high elevation tropical site.**

**However, the conclusions drawn about new particle formation and growth probably need to be revised with a more detailed discussion of diurnal advection processes.**

**The authors mention and discuss large and small scale atmospheric dynamics in section 2.2 and show picture of an advection pathways (fig. 1). That’s important for this study. But, unfortunately the impact of the local diurnal advection processes on the aerosol composition at the site mentioned in sections 4.3 and 4.4 is not further discussed despite the clear statement in section 4.3: “It’s noteworthy that, at high altitudes, the conditions of spatially homogeneous air masses and a steady state, necessary to calculate a realistic growth rate are not verified since air masses are progressively advected to the site from lower altitudes”.**

**The site is located on top of a 12 km long and 700 m high concave volcanic ridge which is opening to the east. This is a perfect textbook location of an orographic structure for the production of early morning thermals. With these thermals air parcels from either Le Port or from St. Andre arrive at the station about two hours after sunrise, depending on the thermal intensity and well in agreement with the observation the appearance of particles at the site (fig. 10). The site is thus a perfect location for an advection study of particles produced elsewhere, most likely close to the coastline. But, that would require to characterize in more detail the thermal upwinds and to relate these to the aerosol and other meteorological data and also to discuss the sources and characteristics of ultrafine particles with the upwind areas.**

AR1-1: We agree that the Maïdo Observatory is the perfect location for the production of early morning thermals. Unfortunately, we do not have the data to analyse in detail thermal upwinds, but we now added a BL tracer diurnal variations for different seasons, which allows us to further discuss the role of BL air advection to the site.

**SC1-2: Sources for emissions of primary ultrafine particles in these locations besides traffic are shipping activities in the port (Le Port), a diesel fired power station in Le Port and probably emissions of a sugar refinery and thermal power station in St. Andre. It's well known that such sources emit particles in the nucleation mode sizes, not only from fossil fuel burning but also from sugar refining. New particle formation via gas to particle conversion during transport naturally cannot be excluded. However, according to Kulmala et al (2013) such a process would take several hours, most likely far more than the two hours of fig. 10 until these new particles would be visible in the SMPS data.**

AR1-2: Because nucleation mode particles precede the accumulation particles that are representative of BL air parcels, we believe that nucleation is initiated during transport and it not already present in the BL before being advected to the site. This is now mentioned in the text. The origin of the precursors is still unknown though and would indeed need more investigations.

**SC1-3: Comparing diurnal patterns of water vapor data from meteorological stations at Le Port or St. Andre and Maido and possibly potential temperature calculated from the in situ temperature at Maido could be helpful for further analysis.**

AR1-3: This is a good suggestion, but we now use BC and  $N_{100}$  as tracers of BL air influence.

# High occurrence of new particle formation events at the Maïdo high altitude observatory (2150 m), Reunion Island (Indian Ocean)

Brice Foucart<sup>1, 2</sup>, Karine Sellegri<sup>2</sup>, Pierre Tulet<sup>1</sup>, Clémence Rose<sup>2</sup>, Jean-Marc Metzger<sup>3</sup>, and David Picard<sup>2</sup>

<sup>1</sup>Laboratoire de l'Atmosphère et des Cyclones (LACy-UMR 8015, CNRS, Université de La Réunion, Météo-France), 97744 Saint Denis de La Réunion, France.

<sup>2</sup>Laboratoire de Météorologie Physique (LaMP-UMR 6016, CNRS, Université Blaise Pascal), 63178, Aubière, France.

<sup>3</sup>Observatoire des Sciences de l'Univers de La Réunion, UMS 3365 (CNRS, Université de La Réunion), 97744 Saint Denis de La Réunion, France.

Correspondence to: Brice Foucart ([brice.foucart@univ-reunion.fr](mailto:brice.foucart@univ-reunion.fr)) and Karine Sellegri ([k.sellegri@opgc.univ-bpclermont.fr](mailto:k.sellegri@opgc.univ-bpclermont.fr))

**Abstract.** This study aims to report and characterize the frequent new particle formation (NPF) events observed at the Maïdo observatory, Reunion Island, a Southern Hemisphere site located at 2150 m (a.s.l.) and surrounded by the Indian Ocean. In 2014 and 2015, continuous aerosol measurements were made using both a Differential Mobility Particle Sizer (DMPS) and an Air Ion Spectrometer (AIS) to characterize the NPF events down to the lowest particle size scale. Carbon monoxide (CO) and Black Carbon (BC) concentrations were monitored, as well as meteorological parameters, in order to identify the conditions that were favourable to the occurrence of nucleation in this specific environment. We point out that the annual NPF frequency average (65%) is one of the highest reported so far. Monthly averages show a bimodal variation of the NPF frequency, with a maximum observed during transition periods (autumn and spring). A high yearly median particle Growth Rate (GR) of 15.16 nm.h<sup>-1</sup> is also measured, occasionally peaking at values of the order of 100 nm.h<sup>-1</sup> and showing a bimodal seasonal variation with maxima observed in July and November. Yearly medians of 2 and 12 nm particle formation rates (J<sub>2</sub> and J<sub>12</sub>) are 0.858 and 0.508 cm<sup>-3</sup>.s<sup>-1</sup> respectively, with a seasonal variation showing a maximum during winter, that correspond to low temperature and RH typical of the dry season, but also to high BC concentrations. We show that the condensation sink exceeds a threshold value (1.04 × 10<sup>-3</sup> s<sup>-1</sup>) with a similar seasonal variation than the one of the NPF event frequency, suggesting that the occurrence of the NPF process might be determined by the availability of condensable vapours, which are likely to be transported together with pre-existing particles from lower altitudes.

## 1 Introduction

Aerosol concentrations in the atmosphere influence the Earth's radiative balance, and the formation and lifetime of clouds (Seinfeld and Pandis, 2016; Makkonen et al., 2012). Unlike the primary sources of aerosols, such as soil erosion, sea salt, and volcanic ash, nucleation is a gas-to-particle conversion process leading to the formation of new secondary aerosol particles. Nucleation and subsequent growth are responsible for New Particle Formation (NPF) events, observed in various environments around the world (Kulmala et al., 2004) but still rarely in the southern hemisphere. The frequency, intensity and duration of NPF events is highly variable according to the location where they are observed. The occurrence and characteristics of NPF episodes depend on various factors,

including the emission strength of precursors, the number concentration of the pre-existing aerosol population, and meteorological parameters (in particular solar radiation, temperature and relative humidity), which directly influence photo-chemical processes (Kulmala, 2003; Martin et al., 2010; Hallar et al., 2016). However, the relationship between these environmental parameters and the characteristics of NPF events is not fully understood and it is still a challenge to predict when an NPF event will take place and how intense it will be (Kulmala et al., 2004; Yu et al., 2008). Consequently, there is still a need to report and describe NPF in environments that have not yet been investigated, notably in the Southern Hemisphere in general and more particularly for both marine and high altitude tropical sites. These kinds of environments present true specificity in terms of RH variability, emission types (Volatile Organic Compounds (VOCs) and Marine sources) and atmospheric dynamics. Previous studies that have been conducted in the Southern Hemisphere relate to South Africa (Hirsikko et al., 2012), with a low latitude-medium altitude (1400 m) site, South America (Rose et al., 2015b) and Australia (Bates et al., 1998), with medium latitude-high altitude sites, and Antarctica (Koponen et al., 2003) as a high latitude area. Hirsikko et al. (2012) published the highest NPF frequency ever reported, of about 86%, explaining that both the local sources (strong mining pollution) and regional conditions affected the NPF variation. Recently, Rose et al. (2015b) proposed a low-latitude zone analysis of NPF at Chacaltaya (CHC) in Bolivia, which is one of the highest in situ measurement sites in the world (5240 m). They, too, found a very high NPF frequency, of about 63.9%. This value has been partly explained by lower concentrations of pre-existing particles than at lower altitudes, leading to smaller loss of gaseous precursors, while photochemical activity is enhanced by higher radiation. In addition, at high altitude stations, turbulence at the interface between the Boundary Layer (BL) and the Free Troposphere (FT) might promote nucleation and growth processes (Hamburger et al., 2011). In general, high altitude sites report relatively high NPF event frequencies, such as 35% at Nepal Climate Observatory (5079 m; Venzac et al., 2008) or 35.9% at the Puy de Dôme station (1465 m; Boulon et al., 2011a). Reunion Island, which is located at low latitude (21 °S) in an inter-tropical area surrounded by the Indian Ocean, is still poorly documented. The island, which was partly shaped by the active basaltic volcano of Piton de la Fournaise (PdF), is characterized by angular landforms and steep slopes. The interaction of the high mountainous terrain with the synoptic flow induces large variability in wind fields at local scale. The maritime and tropical location of the island combined with the complexity of the terrain and wind exposure implies a multitude of local circulations and weather, marked by large variations in temperature and precipitation. This complex atmospheric dynamics added to a large variety of primary and secondary NPF sources (marine, organic and anthropogenic) gives special interest to this study. The Maïdo observatory is located at 2150 m a.s.l., under the influence of the marine boundary layer during daytime and of the free troposphere during nighttime. The main objective of this study is to reinforce the observations of NPF events in the Southern Hemisphere and more particularly for a site that is both marine and at high altitude. We first describe how NPF was observed at the site by DMPS and AIS interpolation (Sect. 4.1.). Based on a multiyear data set of clusters and aerosol size distributions, we secondly report the frequency (Sect. 4.2.), the intensity (Sect. 4.3.) and the characteristics of the events, and describe their seasonality. Thirdly, we analyse their annual variations with respect to the meteorological parameters (Sect. 4.4) and the pre-existing particle concentration (Sect. 4.5.).

## 2 Characteristics of the Maïdo observatory

### 2.1 Geographical location and networks

Maïdo observatory (21.080° S 55.383° E) is situated on La Reunion Island in the Indian Ocean. There are very few multi-instrumented stations in the tropics, and particularly in the southern hemisphere (Baray et al., 2013), so the Maïdo observatory was built in 2012 to respond to the needs of major international networks like NDACC (Network for the Detection of Atmospheric Composition Change, <http://www.ndacc.org>) and ACTRIS (Aerosols, Clouds, and Trace gases Research Infra-Structure network). It is a high-altitude station (2150 m), which opens up new perspectives in upper troposphere and lower stratosphere studies. Belonging to the Global Atmosphere Watch regional network (GAW), it also conducts in situ measurements to characterize the atmospheric composition of the lower troposphere. The facility dominates, in the east, the natural amphitheatre of Mafate, characterized by lush tropical vegetation, and, in the west, the highland tamarind forests. The nearest urban areas are the coastal cities of Saint Paul and Le Port with 105.000 and 40.000 inhabitants respectively, located 13 and 15 km away from the Maïdo observatory (Fig. 1).

### 2.2 Large and local scale atmospheric dynamics

At a large scale, the island is located in the descending part of the South Hadley cell (Baldy et al., 1996). It is subject to the intertropical zone atmospheric circulation, which is characterized by a trade wind flow from the south-east in this lower layer, induced by the Hadley cell and accentuated by more zonal driving by the Walker circulation. This lower layer flow is limited in altitude (about 3 km) by westerly winds (westerlies), which constitute the return of the Hadley – Walker circulation. In terms of rainfall, Reunion Island is characterized by two seasons: the hot, wet season from January to March (southern summer) and the cold, dry season (southern winter), which is longer, lasting from May to November (Baray et al., 2013). April and December are transition months that can be rainy or dry. In the southern summer, the Inter-Tropical Convergence Zone (ITCZ) is situated in the southern hemisphere and sometimes reaches Reunion Island. Over the inversion layer, the westerly flow (between 30°N and 30°S) and west winds weaken and are strongly affected by the context of heavy rains. During the southern winter, the subtropical high pressures are more powerful than during the southern summer and maintain the synoptic subsidence (descending branch of the Hadley cell) that generates and feeds both the stream of faster moving trade winds on the Mascarene region and the subtropical jet at high altitudes.

On a local scale, it is possible to observe two major atmospheric phenomena on both sides of the island. Trade winds coming from the south-east are separated (Fig.1) by the high topography of Reunion, which acts as an obstacle (Lesouëf et al., 2011). They are confined under the inversion layer and forced to bypass the island, forming two branches (Soler, 2000). During the day, a returning loop (Fig. 1) forms in the north-east when the winds converge. The inversion of the circulation then brings the winds under the cities of Saint Paul and Le Port up to the heights towards the Maïdo station. Moreover, the interaction between the trade winds and the abrupt relief of Reunion creates strong climate asymmetry and many microclimates. The warming of mountain slopes by solar radiation during the day, or radiative cooling overnight, is transmitted to the surrounding air layers and creates a complex local circulation. The nocturnal surface radiative cooling induces a cold katabatic wind on the slopes and clears the atmosphere at the Maïdo station, leaving the observatory in the free troposphere, disconnected from the

anthropogenic pollution. Thus there are few clouds during the nighttime. After midday, the sea breeze cumulated in the returning loop wind direction generates upward winds on the slopes which transport particles to the high station, accompanied by orographic and slope cloud formation. The surface radiative warming tends to create convection and then form vertical clouds located at the top of the relief. The number of nights with clear sky is then very large in comparison with the coastal site of Saint Denis, where LIDARs were operated from 1994 to 2011 (Baray et al., 2013).

### 2.3 Volcanic activity

Several studies have provided evidence that high  $\text{SO}_2$  concentrations and high radiation levels favour the formation of large amounts of  $\text{H}_2\text{SO}_4$ , which in turn contribute to particle formation (Hyvönen et al., 2005; Mikkonen et al., 2006; Petäjä et al., 2009) and growth (Boy et al., 2005; Sihto et al., 2006; Mikkonen et al., 2011). Except for some altitude cases where the role of sulfuric acid in nucleation is limited (Boulon et al., 2011a; Rose et al., 2015b; Bianchi et al., 2016),  $\text{H}_2\text{SO}_4$  is thought to be among the major precursors of NPF due to its low saturating vapour pressure under conventional atmospheric temperature conditions (Kulmala and Kerminen, 2008). The Maïdo observatory can be on the pathway of sporadic  $\text{SO}_2$  volcanic plumes emitted from the Piton de la Fournaise (PdF) volcano, located in the south of the island (Fig 1). In 2015, four eruptions were observed (Peltier et al., 2016) and multidisciplinary tracking of a volcanic gas and aerosol plume was conducted by Tulet et al., 2017. Unfortunately,  $\text{H}_2\text{SO}_4$  was not measured but their results indicated that the Maïdo station was reached by the plume several times, as evidenced by the detection of  $\text{SO}_2$  concentration peaks (Fig. A1). Specifically in a volcanic plume environment, Boulon et al. (2011b) directly observed NPF events within the Eyjafjallajökull volcanic plume that reached the Puy de Dôme station, and related them to the presence of high  $\text{H}_2\text{SO}_4$  concentrations. During the PdF eruption that took place in April 2007, Tulet and Villeneuve (2011) used OMI and CALIOP space sensor data to estimate a total  $\text{SO}_2$  release of 230 kt, 60 kt of which was transformed into  $\text{H}_2\text{SO}_4$ , mostly above the Indian ocean, at 6 km a.s.l. As a first analysis, we focus on the parameters influencing new particle formation (NPF) processes at the Maïdo station outside the very specific conditions encountered during a volcanic plume advection, which will be the topic of a separate study. Data were therefore screened for the presence of the Piton de la Fournaise plume at the station. The volcanic plume was considered to be present when the  $\text{SO}_2$  concentration reached values higher than 1 ppb (hourly average), which is the 97th percentile estimated on non-eruptive days. According to Boulon et al. (2011b), this threshold also represented a lower limit of the presence of the plume at the Puy de Dôme station. Consequently, 47 daytime plume days that occurred during three eruptive periods (Fig. A1) were listed and removed from the 2015 data set.

### 2.4 Instrumentation

The aerosol and ion size distributions used in the present study were measured continuously from 01 January to 31 December 2015 at the Maïdo observatory. The size distribution of the 10-500 nm aerosol particles was measured with a Differential Mobility Particle Sizer (DMPS) while the size distribution of the 0.8-42 nm ions was measured with an Air Ion Spectrometer (AIS). Here we use ion size distributions below 10 nm as tracers for the presence of neutral sub-10 nm particles that could not be detected directly. Additional DMPS measurements conducted between May and December 2014 will also be discussed briefly in section 4.1 to evaluate the inter-annual variability of the nucleation frequency.

The DMPS was custom-built with a TSI-type Differential Mobility Analyzer (DMA) operating in a closed loop and a Condensation Particle Counter (CPC, TSI model 3010). Particles were charged to equilibrium using an Ni-63 bipolar charger at 95 MBq. The quality of the DMPS measurements was checked for flow rates and RH according to the ACTRIS recommendations (Wiedensohler et al., 2012). DMPS measurements were performed  
155 down a Whole Air Inlet with a higher size cut-off of 25  $\mu\text{m}$  (under average wind speed conditions of 4  $\text{m}\cdot\text{s}^{-1}$ ).

The AIS was developed by Airel, Estonia, for in situ high time resolution measurements of ions and charged particles (Mäkelä et al., 1996 and Mirme et al., 2007). The device consists of two DMA arranged in parallel, which allows the simultaneous measurement of both negatively and positively charged particles. Each of the two analysers operates with a total flow of 90 litres per minute (lpm): 30 lpm of air to be sampled and 60 lpm of clean  
160 air (or carrier gas) circulating in closed loop. The AIS was directly connected to ambient air through a 30 cm long copper inlet 2.5 cm in diameter, to limit cluster ion losses along the sampling line.

The global radiation was measured using a Sunshine Pyranometer (SPN1, Delta-T Devices Ltd.) with a resolution of 0.6  $\text{W}\cdot\text{m}^{-2}$ . The auxiliary measurements used in the present study were the wind direction, the wind speed, the air temperature, the barometric pressure and the relative humidity. They were measured using the Vaisala Weather  
165 Transmitter WXT510 (<http://www.vaisala.com>).

The analyser used to measure sulfur dioxide ( $\text{SO}_2$ ) concentrations uses the ultraviolet fluorescence method, standard NF EN 14212. The molecules are excited under the action of intense, constant UV radiation (214 nm). Sulfur dioxide then de-energizes very quickly by emitting higher wavelength radiation (between 320 and 380 nm) than the excitation step.  $\text{SO}_2$  concentration was finally calculated by means of a photomultiplier. Datasets were  
170 provided by the Observatoire Réunionnais de l'Air (ORA). The  $\text{SO}_2$  analyser resolution was about 0.5 ppb and, outside eruptive periods, it never exceeded this threshold (Fig. A1). The corresponding data were used only to list days that were characterized by the presence of the volcanic plume at the Maïdo observatory.

CO monitoring was performed using a PICARRO G2401 analyzer which is compliant with international ambient atmospheric monitoring networks, including the World Meteorological Organization (WMO) and the Integrated  
175 Carbon Observation System (ICOS, <https://www.icos-ri.eu/>). It was the property of BIRA-IASB (Belgian Institute for Space Aeronomy).

Figure 3 shows the availability of data for the main aerosol and gas-phase parameters used in this study. The best instrument synchronization period was from May to November.

### 3 Calculations

180 The classification of event days was achieved visually using the contour plot of the DMPS size distribution. The positive and negative ion size distributions provided by the AIS confirmed the status of the event when available. Days were classified and separated into three main groups: undefined, ( $UN$ ) non-event ( $NE$ ) and event ( $E$ ) days according to Dal Maso et al. (2005).

The monthly event frequency,  $f_m$ , was calculated as the ratio of event to non-event days, after having excluded  
185 undefined, missing and plume days ( $PD$ ), according to Eq. (1):

$$f_m = \frac{\text{number of } E}{\text{number of days in month} - (\text{missing data days} + PD)} \times 100, \quad (1)$$

The condensation sink (CS;  $s^{-1}$ ), which represents the loss rate of vapours on pre-existing particles was calculated from the DMPS size distributions according to Kulmala et al.'s (2001a) Equation (2):

$$CS = 4\pi D_{vap} \int_0^{\infty} r\beta(r)N(r)dr \quad (2)$$

190 where  $D_{vap}$  is the condensable vapour diffusion coefficient,  $r$  the particle radius and  $N(r)$  the concentration of particles of radius  $r$ . Coefficient  $\beta(r)$  was calculated from the Knudsen number and is given by Eq. (3):

$$\beta(r) = \frac{1+Kn(r)}{1+Kn(r)\left(\frac{4}{3\alpha}+0.337\right)+\frac{4}{3\alpha}Kn(r)^2} \quad (3)$$

where  $Kn(r)$  is the Knudsen number given by  $Kn(r) = \lambda / r$ , with  $\lambda$  corresponding to the particle free path (depending on pressure and temperature) and the accommodation coefficient  $\alpha$ , usually set at 1. The condensation  
195 sink was calculated with a five minute time resolution. As the particles are dried in the DMPS, we are aware that the CS, which depends on the diameter of wet particles, was underestimated.

The particle growth rate (GR;  $nm.h^{-1}$ ) was determined using the "maxima" method of Hirsikko et al. (2005). The method searches, usually over the AIS channel size, for the time that corresponds to the maximum concentration in each size channel. As the DMPS offers a much more extended data set than the AIS, we applied the method to  
200 the DMPS 12-19 nm size range for which the lower limit (12) was defined by the smallest channel of the device.

In order to detect the concentration maximum, a normal distribution was fitted to the time evolution of the concentration for each channel. GR corresponded to the slope of the linear regression on the time-diameter pairs. The formation rate of 12 nm particles,  $J_{12}$ , ( $cm^{-3}.s^{-1}$ ) was calculated using the following Equation (4) given by Kulmala et al. (2007):

$$205 \quad J_{12} = \frac{dN_{12-19}}{dt} + CoagS_{12} \times N_{12-19} + \frac{GR_{12-19}}{7 \text{ nm}} \times N_{12-19} \quad (4)$$

where  $N_{12-19}$  is the concentration corresponding to 12 to 19 nm particle diameters,  $CoagS_{12}$  represents the coagulation of 12 nm particles on pre-existing larger diameter particles and  $GR_{12-19}$  corresponds to the growth rate estimated between 12 and 19 nm. It was then possible to derive the nucleation rates of particles 2 nm in size,  $J_2$ , from the  $J_{12}$  previously calculated from DMPS and the growth rate of particles between 12 and 19 nm, following  
210 the method first introduced by Kerminen and Kulmala (2002) and improved by Lehtinen et al. (2007) with Eq. (5):

$$J_2 = \frac{J_{12}}{\exp\left(-\gamma \times d_2 \times \frac{CoagS(d_2)}{GR_{12-19}}\right)} \quad (5)$$

where,

$$\gamma = \frac{1}{m+1} \left[ \left( \frac{d_{12}}{d_2} \right)^{m+1} - 1 \right] \quad (6)$$

and,

$$215 \quad m = \frac{\log(CoagS(d_{12})) - \log(CoagS(d_2))}{\log(d_{12}) - \log(d_2)} \quad (7)$$

## 4 Results and discussion

### 4.1 Dynamics of the NPF events at the Maïdo observatory

The origin of the newly formed particles at a given site can be attributed to the local environment only if newly formed particles are detected at the smallest size range, when clusters just formed and had no time yet to grow. Thus, we used both the AIS and DMPS size distribution to investigate the evolution of NPF event at Maïdo. The AIS covers the size range between 0.90 and 46.2 nm while the DMPS covers the size range between 11.78 and 706.77 nm. Temporal interpolation was first performed to harmonize the DMPS and the AIS data sets to a 5 min resolution. For visual inspection of the consistency of the two data sets, hybrid plots were drawn up showing the AIS negative ion concentration up to 12 nm and then the particle concentration from the DMPS for larger sizes. Figure 3a shows an example of an NPF event followed by the two devices on 06 July, 2015. Typically, NPF events observed at the Maïdo observatory show an increase of small ion concentrations (2-5 nm) at dawn (06:00 UTC, corresponding to 10:00 LT). These small ions are tracers for small particles of the same size that rapidly grow to the first DMPS size classes within the next hour. The initiation of the formation of new particles at 06:00 UTC (10:00 LT) is followed by the appearance of accumulation mode particles. Further growth of the newly formed particles is generally accompanied by the simultaneous growth of the accumulation mode particles, starting around 07:00 UTC (11:00 LT), that are likely representative of the updraft of boundary layer air to the station. We computed the diurnal variation of black carbon (BC), a good indicator of any anthropogenic, hence boundary layer, influence. The corresponding diurnal variation of BC ( $\text{ng.m}^{-3}$ ) is shown on Figure 3b. BC concentration clearly increases from 06:30 UTC (when ignoring early sharp peaks that may due to local contamination), which is half an hour later than the occurrence of the cluster mode particles. Hence we can hypothesise that boundary air convection to the site is a trigger for NPF events, most particularly when the interface BL/FT is sampled. At 07:00 UTC, as the accumulation particle concentration increase from 2000 to 8000  $\text{part.cm}^{-3}$ , the BC concentration also increase to reach 630  $\text{ng.m}^{-3}$  at 09:00, when the BL is fully sampled at the site. At the end of the afternoon, the accumulation mode particles concentrations drop to less than 1000  $\text{particle.cm}^{-3}$  and BC concentrations drop to very low values. Most high altitude stations are strongly influenced by free troposphere air during nighttime regardless the season, but mostly during wintertime (Venzac et al., 2008; Rose et al., 2015a). This is also true for stations located in complex terrains such as Jungfrauoch station in the Swiss Alps (Herrmann et al., 2015) and at the Chacaltaya station in the Andes (Rose et al., 2015b). These are indicators that the station lays in the free troposphere at night. The Aitken mode particles present during nighttime at the station are hence likely present in the free troposphere and are sampled at the site in subsiding air masses (Tulet et al., 2017). These features can also be observed on average, both for the summer and winter seasons. BC average diurnal profiles (a), together with the average diurnal variation of the number concentrations of particles larger than 100 nm ( $N_{100}$ ) (b), and the number concentration of nucleation mode particles with a diameter smaller than 30 nm ( $N_{30}$ ) (c) are shown on Figure 4. We observe that, on average, BC concentrations increase in the morning at the same time as  $N_{100}$  and  $N_{30}$ , confirming the influence of the BL on the occurrence of NPF events at the scale of the season. Moreover, we can note that during winter, BC concentrations are higher during nighttime (from 16:00 to 06:00 UTC) than during summer. This observation is also true for  $N_{100}$  with higher values from 17:00 to 02:00 UTC during winter compared to summer. We assume that during winter, trade winds favour the large scale remote primary particles transport to the Maïdo station.

#### 255 4.2 Nucleation and frequency analysis

Over the measurement period in 2015, 47 volcanic plume days were excluded and data was missing on 61 days. Among the 257 remaining days, 167 days (65%) were classified as event days, 55 (21%) as non-event days and 35 (14%) as undefined. As a result, the event frequency was high for the Maïdo station, with an annual average of 65% (med: 65.2%; 25ile: 52.0%; 75ile: 80.0%) for 2015. This frequency is one of the highest values reported so far, with the exceptions of the South African plateau, where NPF was reported to occur 86% of the time according to (Hirsikko et al., 2012), and savannah, with 69% of the time (Vakkari et al., 2011). Figure 5 shows the seasonal variation of the monthly event frequency,  $f_m$ .

As shown in Figure 5, similar seasonal variations were observed for the nucleation frequency in 2014 and part of 2015. High NPF frequencies were observed during the transition months being on average 72.5% for October and November (spring), and even slightly higher, 89.4%, for March to May (autumn). During the southern winter and summer seasons (from June to August and from January to February), NPF was lower. As examples of high and low frequency NPF months, continuous DMPS spectra of April (93.1% occ.) and June (46.7% occ.) are available in the supplementary section though (Figure A4).

### 4.3 Particle formation, growth and nucleation rates

The yearly average particle growth rate for 12-19 nm particles was  $19.4 \pm 12.69$  nm.h<sup>-1</sup> (Table 1), which is above the typical range of GRs reported in the literature for a quite-similar size class of 7-20 nm (GR<sub>7-20</sub>). The review by Yli-Juuti et al. (2011) of GR<sub>7-20</sub>, obtained at different measurement sites located in various environments, reports a yearly average of  $6.66 \pm 3.41$  nm.h<sup>-1</sup> (19 values). However, higher GRs have been observed for a coastal environment in Australia, with an average GR<sub>7-20</sub> of 19 nm.h<sup>-1</sup>, (Modini et al., 2009) and for a polluted urban environment in Tecamac, with an 18 nm.h<sup>-1</sup> average GR<sub>3,7-25</sub> (Iida et al., 2008). It is noteworthy that, at high altitudes, the conditions of spatially homogeneous air masses and a steady state, necessary to calculate a realistic growth rate, are not verified since air masses are progressively advected to the site from lower altitudes. Thus the GRs that are reported here are “apparent” growth rates that may be overestimated due to the transport of particles that have already nucleated and grown at lower altitudes at the same time. Nevertheless, the particle GR calculated for the Maïdo station is higher than the average GRs reported by Rose et al. (2015b) for the CHC station (7.62 nm.h<sup>-1</sup>), Boulon et al. (2011a) for the Puy-de-Dôme station (6.20 nm.h<sup>-1</sup>), and Venzac et al. (2008) for Nepal (1.8 nm.h<sup>-1</sup>).

In our calculation, 19 events were not taken into account because of the special characteristics of the extreme value of GR. The beginning of the NPF was characterized by a clear verticality in the spectrum during the first hours of the event and the corresponding GR was generally very high (100 to 150 nm.h<sup>-1</sup>). Two examples of DMPS spectra belonging to this special class of growth rates are shown on Figure A2. Most of them were observed in December (8 cases). Dal Maso (2002) and O’Dowd and De Leeuw (2007) obtained such values (100 nm.h<sup>-1</sup>) at Mace Head, a coastal site in western Ireland. They can be explained by the simultaneous transport of nucleated and already grown particles to the sampling site, from seaweed fields. In the case of coastal marine NPF events, the spatial homogeneity of the emission field is not verified, as for high altitude sites.

Figure 6 highlights a clear seasonal variation of GR<sub>12-19</sub>, with the highest monthly averages in August (35 nm.h<sup>-1</sup>) and the lowest in May (8.9 nm.h<sup>-1</sup>). These variations of the GR differ from those reported in the literature for other high altitude sites. Boulon et al. (2011a), did not find a significant seasonal pattern in the GR variation at the Puy de Dôme. In Chacaltaya, Rose et al. (2015b) showed that, on average, the GRs were enhanced during the wet

295 period, which is not in agreement with the present study, as we find high medians during the dry period (22.82 nm.h<sup>-1</sup> averaged from July to November). Several reasons may explain these discrepancies, such as the topography of each station relative to cloud location during the wet season or the seasonal variation of condensable species responsible for the particle growth.

Formation rates were calculated for 12 and 2 nm particles when the GR<sub>12-19</sub> was available. The yearly average formation rates J<sub>12</sub> and J<sub>2</sub> in Table 1 are respectively 0.931 ±1.15 and 1.53 ±2.06 cm<sup>-3</sup>.s<sup>-1</sup>. These formation rates are in the upper range of the values reported by Kulmala et al. (2004) from measurements performed in more than 100 locations in the boundary layer (J<sub>3</sub> = 0.01-10 cm<sup>-3</sup>.s<sup>-1</sup>). They are of the same order of magnitude as the ones reported for the CHC (1.02 and 1.90 cm<sup>-3</sup>.s<sup>-1</sup> for the wet and dry seasons respectively, (Rose et al., 2015b).

J<sub>2</sub> seasonal variation follows the J<sub>12</sub> seasonal variation (Fig. 7) but with higher values due to losses by coagulation during the growth process. We observe a clear seasonal cycle with maximum values during the dry season, particularly between July and September (J<sub>12</sub> = 1.60 cm<sup>-3</sup>.s<sup>-1</sup> and J<sub>2</sub> = 2.39 cm<sup>-3</sup>.s<sup>-1</sup> respectively, averaged over 3 months). These observations are consistent with those reported for CHC, where J<sub>2</sub> were reported to be twice as high during the dry season as in the wet season (Rose et al., 2015b). The lowest values are obtained around the transition months of December, with J<sub>12</sub> = 0.32 cm<sup>-3</sup>.s<sup>-1</sup> and J<sub>2</sub> = 0.52 cm<sup>-3</sup>.s<sup>-1</sup> (averaged between November and 310 January), and April, with J<sub>12</sub> = 0.44 cm<sup>-3</sup>.s<sup>-1</sup> and J<sub>2</sub> = 0.66 cm<sup>-3</sup>.s<sup>-1</sup> (averaged between April to June). The seasonal variation of the growth rate reported in Figure 6 also shows highest values around August but the seasonal variation of nucleation rates shows features different from those of the GR. Formation rates reach their maxima slightly earlier in the dry season (July) than the growth rates, and the contrast between July-August-Sept and the rest of the year is also stronger. This indicates that the condensable vapours necessary for nucleating new particles might not have exactly the same seasonal variation as the ones required for growing the newly formed particles. In addition, high particle formation and growth rates obtained in July-August do not coincide with the highest nucleation frequencies, suggesting that, during these months, NPF might be less frequent but occur in the form of stronger events.

Several factors have previously been reported to influence the seasonal variation of the NPF event frequency, GR, and nucleation rates; they include (i) the availability of condensable gases involved in the formation of new particles, (ii) the number concentration of pre-existing particles transported to the site and (iii) thermo-dynamical properties of the atmosphere, such as radiation, temperature, and relative humidity. In the following sections, we will explore the seasonal variation of the last two factors (ii and iii).

#### 4.4 Meteorological parameters and onset of NPF

325 A summary of incidental radiation, relative humidity, temperature and pressure monthly averages is available in Table A1. Austral seasons are reflected regarding both the daily averaged temperature and radiation represented on Figure 8a. We also computed in Table 2 the existing relationships between the monthly average meteorological parameters and the ones of the main characteristics of the NPF events. We observe that radiation is highest between September and November (272.19 W.m<sup>-2</sup> on average), coinciding with one period of high NPF frequency (Fig. 4), but not with the maximum frequency of occurrence (March to May), nor with any high values of the GR or J<sub>2</sub>/J<sub>12</sub> (Figs. 6 and 7). As a consequence, no correlation is observed between radiation and the NPF variables. Hence, the availability of light for photochemistry is not the only parameter influencing the NPF frequency, nor the formation rates or growth. The temperature averages are higher from November to April (14.02 °C). We find a significant

(at the 95% confidence level) anti-correlation between temperature and the nucleation rate and GR. However, the seasonal temperature variations are similar to the seasonal variation of the NPF event frequency even if the correlation is not significant at the 95% confidence level. Emissions of terpenes is favoured at higher temperatures (Yu et al., 2017) while higher radiation is favouring the isoprene emissions. Some studies have shown that high concentration of isoprene relative to monoterpene can inhibit new particle formation while favouring particle growth (Kiendler-Scharr et al., 2009; Kanawade et al., 2011; Freney et al., 2017). This effect could partly explain that higher temperatures favour the nucleation frequency occurrence but lead to lower growth rates. Other factors such as a direct effect of temperature on the saturation vapour pressure of condensable gases can also influence this result.

The relative humidity values are typical of an inter-tropical island with peaks in summer, between December and March (76.79% on average), and the lowest values obtained in July and September. Cloudy conditions were previously shown to inhibit formation of new particles, by scavenging newly formed clusters (Venzac et al., 2007). They might also decrease photochemical processes at the origin of the formation of condensable species contributing to the growth of clusters to stable particles. At Chacaltaya, Bolivia (5200 m a.s.l), Rose et al. (2015b) reported high frequencies during the southern winter, which coincide with the dry season. For the Maïdo station, frequency variations are not fully synchronized with the dry or wet periods as defined in Fig 8b. However, there is some uncertainty both in the dry/wet season segregation and with the exact identification of maxima/minima in the seasonal variation of the NPF frequency. When considering relative humidity, we do not find any link between RH and the nucleation frequency (Table 2) but a significant anti-correlation with the formation rate: low RH values correspond to the July-August-September nucleation peak. This would be in agreement with the results from the CHC station. Figure 8b shows that the appearance time of the ultrafine particles seasonal variation is well correlated to the sunrise. During the southern summer, NPF starts between approximately 08:00 and 10:00 LT and between 09:00 and 10:00 during the southern winter. This correlation may be due to the need for sunlight to be available to start photochemical processes, or/and to the start of advection of precursor gases from lower altitude sources in the BL.

#### 4.5 Condensation sink

In addition to the meteorological parameters, the seasonal variation of the NPF characteristics might also be influenced by the presence of pre-existing particles, known to inhibit the NPF processes by increasing the competition for available condensable gases. We averaged the CS for two hours before the nucleation started (CS<sub>2</sub>) to properly characterize its influence on the occurrence of an NPF event. In Figure 8b, nucleation onset times are averaged for each season (08:00 LT for southern summer and 09:00 LT for southern winter). The yearly average condensation sink has been calculated to be  $2.43 \times 10^{-3} \text{ s}^{-1}$  and  $1.86 \times 10^{-3} \text{ s}^{-1}$  for CS<sub>2</sub>. These values are similar to the ones reported for the altitude station of Chacaltaya (Rose et al., 2015b) and Nepal (Venzac et al., 2008) which are  $2.4 \times 10^{-3} \text{ s}^{-1}$  and  $2.1 \times 10^{-3} \text{ s}^{-1}$  respectively and also for the Mace Head coastal station (Dal Maso, 2002) which is about  $2 \times 10^{-3} \text{ s}^{-1}$ .

Monthly averages of the CS<sub>2</sub> were calculated for event days and non-event days and are shown for 2015 on Figure 9a, together with the NPF event monthly frequency  $f_m$ . This representation highlights monthly averaged CS<sub>2</sub> peaks for February ( $2.65 \times 10^{-3} \text{ s}^{-1}$ ), May ( $3.74 \times 10^{-3} \text{ s}^{-1}$ ) and September ( $4.72 \times 10^{-3} \text{ s}^{-1}$ ). The September value is similar to the South African savannah yearly average (Vakkari et al., 2011), which was about  $4.3 \times 10^{-3} \text{ s}^{-1}$ . It attests to a

considerable presence of pre-existing particles at the Maïdo station for this period. However, the NPF frequency seasonal pattern does not match that of low CS<sub>2</sub>. May and September CS<sub>2</sub> peaks are associated with  $f_m$  peak values while January and June CS<sub>2</sub> low averages ( $0.89$  and  $0.96 \times 10^{-3} \text{ s}^{-1}$  respectively) are correlated to weak NPF occurrence.

Moreover, we calculated that the annual CS<sub>2ev</sub> (event) median ( $1.2 \times 10^{-3} \text{ s}^{-1}$ ) was significantly higher than the annual CS<sub>2noev</sub> (no event) median ( $8.5 \times 10^{-4} \text{ s}^{-1}$ ). The previous observations thus suggest that the condensation sink does not inhibit NPF at Maïdo, as previously reported for other high altitude stations (Manninen et al., 2010; Boulon et al., 2010; Rose et al., 2015a). At these sites, the occurrence of the NPF process might be determined rather by the availability of condensable vapours, which are likely to be transported together with pre-existing particles from lower altitudes. In order to further investigate this aspect, we evaluated whether the frequency of nucleation was correlated to a frequency of exceeding a CS threshold. Hence, we calculated a monthly average frequency for which the CS<sub>2</sub> exceeded a threshold value of  $1.04 \times 10^{-3} \text{ s}^{-1}$ . The threshold was chosen arbitrarily as a value intermediate between the annual CS<sub>2ev</sub> and CS<sub>2noev</sub> medians. We started our investigation by choosing the median CS over the whole year as a threshold value. We then used an iteration process to fix the threshold so we have a reasonable seasonal variation of days exceeding this threshold values. Choosing other threshold values within CS<sub>2ev</sub> and CS<sub>2noev</sub> medians range would have led to less pronounced variability but would not have changed the shape of the seasonal trend. The resulting frequency at which CS<sub>2</sub> exceeded the threshold (Fig. 9b) had a clear seasonal variation with maxima during the transitional periods. For April-May, and September-November, more than 60% of the CS<sub>2</sub> were higher than  $1.04 \times 10^{-3} \text{ s}^{-1}$ , while for January, June and July the frequency was lowest. Hence, we actually find a similar seasonal variation between the frequency of CS exceeding a threshold value and the frequency of occurrence of NPF events (also shown by Table 2). This strengthens the hypothesis that there are precursors potentially transported simultaneous to aerosols from lower altitudes.

#### 4.6 Black Carbon as a tracer of the anthropogenic contribution

Potential precursors may be of anthropogenic origin and we investigated their potential contribution by using BC as a tracer. Figure 10a and 10b show the monthly mean concentrations of BC and CO over the year 2015. The best similarity between the seasonal variations of BC and the ones of NPF parameters is found for the nucleation rate (Table 2). This may indicate that air masses influenced by a larger contribution of anthropogenic compounds are favourable to more intense NPF events, but not necessarily more frequent. Indeed, moderately high NPF frequencies are observed for high BC monthly mean values during the spring period, but the high frequencies of NPF event occurrence observed during the autumn period are not associated to very large BC monthly mean concentrations, and thus other contributors are expected during autumn. The growth rate of newly formed particles is best correlated to CO concentrations (Table 2). This suggests that CO and BC do not have the exact same sources. Co may originate from other sources than combustion process, such as marine source. This result also confirms that condensable species necessary to form new particles are hence likely different from the ones responsible for their further growth.

## 5 Conclusions

In the present study, we provide a new NPF observations for a high altitude site of the southern hemisphere, the Maïdo observatory. We report a remarkably high frequency of occurrence of NPF events at the Maïdo observatory

(65%) with a bimodal seasonal variation of this frequency, characterized by high values during spring and autumn. We show that the condensation sink exceeds a threshold value ( $1.04 \times 10^{-3} \text{ s}^{-1}$ ) with a similar seasonal variation than the one of the NPF event frequency, suggesting that, similarly to other altitude sites, the condensation sink does not inhibit NPF at Maïdo, but the occurrence of the NPF process might be determined rather by the availability of condensable vapours, which are likely to be transported together with pre-existing particles from lower altitudes during the day. This indicates an influence of the boundary layer dynamics, confirmed by daily variations of boundary layer tracers ( $N_{100}$  and BC). The monthly average BC concentrations, taken as one anthropogenic tracer, has a main peak during winter and hence they match only a fraction of NPF frequency. Thus, anthropogenic precursors may contribute to some of the springtime NPF occurrence, but the high NPF occurrence during the autumn season is likely initiated by other contributors. The seasonal variations of the formation rate and growth rate are not correlated to the NPF frequency seasonal variation. High formation rates correspond to high BC concentrations, low relative humidity conditions and low temperatures. While annual average  $J_{12}$  and  $J_2$  are in the typical ranges found in the literature ( $9.31 \times 10^{-2} \pm 1.15$  and  $1.53 \pm 2.06 \text{ cm}^{-3} \cdot \text{s}^{-1}$  respectively),  $GR_{12-19}$  values are higher than the typical range of GRs reported in the literature ( $19.4 \pm 12.69 \text{ nm} \cdot \text{h}^{-1}$ ). At Reunion Island, the identification of different sources contributing to the gas phase composition of the atmosphere is not well established. To complete this work, it would be valuable to have direct measures of the cluster ion composition that would provide indication of the anthropogenic, vegetation or marine sources contributions to nucleation at the site. In addition and although they are complex, modelling methods such as a detailed back-trajectory analysis should be used to understand the origin of the local air masses and source contributions at the Maïdo observatory.

## 430 Acknowledgments

This project has received funding from the European Union's Horizon 2020 research and innovation programme under grant agreement No 654109 (ACTRIS-2), from the French programme SNO-CLAP, and from the OMNCG/OSU-R programme of La Réunion University. We also wish to thank the ORA (Observatoire Réunionnais de l'Air) for providing the  $\text{SO}_2$  dataset as Jean SCIARE who provides the processed data from the aethalometer.

## References

- Baldy, S., Ancellet, G., Bessafi, M., Badr, A. and Luk, D. L. S.: Field observations of the vertical distribution of tropospheric ozone at the island of Reunion (southern tropics), *J. Geophys. Res. Atmospheres*, 101(D19), 23835–23849, doi:10.1029/95JD02929, 1996.
- 440 Baray, J.-L., Courcoux, Y., Keckhut, P., Portafaix, T., Tulet, P., Cammas, J.-P., Hauchecorne, A., Godin-Beekmann, S., De Mazière, M., Hermans, C. and others: Maïdo observatory: a new high-altitude station facility at Reunion Island ( $21^\circ \text{ S}$ ,  $55^\circ \text{ E}$ ) for long-term atmospheric remote sensing and in situ measurements, *Atmospheric Meas. Tech.*, 6(10), 2865–2877, 2013.
- 445 Bates, T. S., Kapustin, V. N., Quinn, P. K., Covert, D. S., Coffman, D. J., Mari, C., Durkee, P. A., De Bruyn, W. J. and Saltzman, E. S.: Processes controlling the distribution of aerosol particles in the lower marine boundary layer during the First Aerosol Characterization Experiment (ACE 1), *J. Geophys. Res. Atmospheres*, 103(D13), 16369–16383, doi:10.1029/97JD03720, 1998.

- 450 Bianchi, F., Tröstl, J., Junninen, H., Frege, C., Henne, S., Hoyle, C. R., Molteni, U., Herrmann, E., Adamov, A., Bukowiecki, N. and others: New particle formation in the free troposphere: A question of chemistry and timing, *Science*, 352(6289), 1109–1112, 2016.
- Boulon, J., Sellegri, K., Venzac, H., Picard, D., Weingartner, E., Wehrle, G., Collaud Coen, M., Bütikofer, R., Flückiger, E., Baltensperger, U. and Laj, P.: New particle formation and ultrafine charged aerosol climatology at a high altitude site in the Alps (Jungfrauoch, 3580 m a.s.l., Switzerland), *Atmospheric Chem. Phys.*, 10(19), 9333–9349, doi:10.5194/acp-10-9333-2010, 2010.
- 455 Boulon, J., Sellegri, K., Hervo, M., Picard, D., Pichon, J.-M., Fréville, P. and Laj, P.: Investigation of nucleation events vertical extent: a long term study at two different altitude sites, *Atmospheric Chem. Phys.*, 11(12), 5625–5639, doi:10.5194/acp-11-5625-2011, 2011a.
- Boulon, J., Sellegri, K., Hervo, M. and Laj, P.: Observations of nucleation of new particles in a volcanic plume, *Proc. Natl. Acad. Sci.*, 108(30), 12223–12226, 2011b.
- 460 Boy, M., Kulmala, M., Ruuskanen, T. M., Pihlatie, M., Reissell, A., Aalto, P. P., Keronen, P., Maso, M. D., Hellen, H., Hakola, H. and others: Sulphuric acid closure and contribution to nucleation mode particle growth, *Atmospheric Chem. Phys.*, 5(4), 863–878, 2005.
- D O’Dowd, C. and De Leeuw, G.: Marine aerosol production: a review of the current knowledge, *Philos. Trans. R. Soc. Lond. Math. Phys. Eng. Sci.*, 365(1856), 1753–1774, 2007.
- 465 Dal Maso, M.: Condensation and coagulation sinks and formation of nucleation mode particles in coastal and boreal forest boundary layers, *J. Geophys. Res.*, 107(D19), doi:10.1029/2001JD001053, 2002.
- 470 Dal Maso, M., Kulmala, M., Riipinen, I., Wagner, R., Hussein, T., Aalto, P. P. and Lehtinen, K. E.: Formation and growth of fresh atmospheric aerosols: eight years of aerosol size distribution data from SMEAR II, Hyytiälä, Finland, *Boreal Environ. Res.*, 10(5), 323, 2005.
- 475 Freney, E., Sellegri, K., Chrit, M., Adachi, K., Brito, J., Waked, A., Borbon, A., Colomb, A., Dupuy, R., Pichon, J.-M., Bouvier, L., Delon, C., Jambert, C., Durand, P., Bourianne, T., Gaimoz, C., Triquet, S., Féron, A., Beekmann, M., Dulac, F. and Sartelet, K.: Aerosol composition and the contribution of SOA formation over Mediterranean forests, *Atmospheric Chem. Phys. Discuss.*, 1–25, doi:10.5194/acp-2017-482, 2017.
- Hallar, A. G., Petersen, R., McCubbin, I. B., Lowenthal, D., Lee, S., Andrews, E. and Yu, F.: Climatology of New Particle Formation and Corresponding Precursors at Storm Peak Laboratory, *Aerosol Air Qual. Res.*, 16(3), 816–826, doi:10.4209/aaqr.2015.05.0341, 2016.
- 480 Hamburger, T., McMeeking, G., Minikin, A., Birmili, W., Dall’Osto, M., O’Dowd, C., Flentje, H., Henzing, B., Junninen, H., Kristensson, A., de Leeuw, G., Stohl, A., Burkhardt, J. F., Coe, H., Krejci, R. and Petzold, A.: Overview of the synoptic and pollution situation over Europe during the EUCAARI-LONGREX field campaign, *Atmospheric Chem. Phys.*, 11(3), 1065–1082, doi:10.5194/acp-11-1065-2011, 2011.
- 485 Herrmann, E., Weingartner, E., Henne, S., Vuilleumier, L., Bukowiecki, N., Steinbacher, M., Conen, F., Collaud Coen, M., Hammer, E. and Jurányi, Z.: Analysis of long-term aerosol size distribution data from Jungfrauoch with emphasis on free tropospheric conditions, cloud influence, and air mass transport, *J. Geophys. Res. Atmospheres*, 120(18), 9459–9480, 2015.

- 490 Hirsikko, A., Laakso, L., Hörrak, U., Aalto, P. P., Kerminen, V. and Kulmala, M.: Annual and size dependent variation of growth rates and ion concentrations in boreal forest, *Boreal Environ. Res.*, 10(5), 357, 2005.
- Hirsikko, A., Vakkari, V., Tiitta, P., Manninen, H. E., Gagné, S., Laakso, H., Kulmala, M., Mirme, A., Mirme, S., Mabaso, D., Beukes, J. P. and Laakso, L.: Characterisation of sub-micron particle number concentrations and formation events in the western Bushveld Igneous Complex, South Africa, *Atmospheric Chem. Phys.*, 12(9), 3951–3967, doi:10.5194/acp-12-3951-2012, 2012.
- 495 Hyvönen, S., Junninen, H., Laakso, L., Dal Maso, M., Grönholm, T., Bonn, B., Keronen, P., Aalto, P., Hiltunen, V., Pohja, T., Launiainen, S., Hari, P., Mannila, H. and Kulmala, M.: A look at aerosol formation using data mining techniques, *Atmos Chem Phys*, 5(12), 3345–3356, doi:10.5194/acp-5-3345-2005, 2005.
- 500 Iida, K., Stolzenburg, M. R., McMurry, P. H. and Smith, J. N.: Estimating nanoparticle growth rates from size-dependent charged fractions: Analysis of new particle formation events in Mexico City, *J. Geophys. Res. Atmospheres*, 113(D5) [online] Available from: <http://onlinelibrary.wiley.com/doi/10.1029/2007JD009260/full> (Accessed 25 August 2017), 2008.
- 505 Kanawade, V. P., Jobson, B. T., Guenther, A. B., Erupe, M. E., Pressley, S. N., Tripathi, S. N. and Lee, S.-H.: Isoprene suppression of new particle formation in a mixed deciduous forest, *Atmospheric Chem. Phys.*, 11(12), 6013–6027, doi:10.5194/acp-11-6013-2011, 2011.
- Kerminen, V.-M. and Kulmala, M.: Analytical formulae connecting the “real” and the “apparent” nucleation rate and the nuclei number concentration for atmospheric nucleation events, *J. Aerosol Sci.*, 33(4), 609–622, doi:10.1016/S0021-8502(01)00194-X, 2002.
- 510 Kiendler-Scharr, A., Wildt, J., Maso, M. D., Hohaus, T., Kleist, E., Mentel, T. F., Tillmann, R., Uerlings, R., Schurr, U. and Wahner, A.: New particle formation in forests inhibited by isoprene emissions, *Nature*, 461(7262), 381–384, doi:10.1038/nature08292, 2009.
- Koponen, I. K., Virkkula, A., Hillamo, R., Kerminen, V.-M. and Kulmala, M.: Number size distributions and concentrations of the continental summer aerosols in Queen Maud Land, Antarctica, *J. Geophys. Res. Atmospheres*, 108(D18) [online] Available from: <http://onlinelibrary.wiley.com/doi/10.1029/2003JD003614/full> (Accessed 24 August 2017), 2003.
- 515 Kulmala, M.: ATMOSPHERIC SCIENCE: How Particles Nucleate and Grow, *Science*, 302(5647), 1000–1001, doi:10.1126/science.1090848, 2003.
- Kulmala, M. and Kerminen, V.-M.: On the formation and growth of atmospheric nanoparticles, *Atmospheric Res.*, 90(2–4), 132–150, doi:10.1016/j.atmosres.2008.01.005, 2008.
- 520 Kulmala, M., Maso, M. D., Mäkelä, J. M., Pirjola, L., Väkevä, M., Aalto, P., Miikkulainen, P., Hämeri, K. and O’ Dowd, C. D.: On the formation, growth and composition of nucleation mode particles, *Tellus B Chem. Phys. Meteorol.*, 53(4), 479–490, doi:10.3402/tellusb.v53i4.16622, 2001.
- 525 Kulmala, M., Vehkamäki, H., Petäjä, T., Dal Maso, M., Lauri, A., Kerminen, V.-M., Birmili, W. and McMurry, P. H.: Formation and growth rates of ultrafine atmospheric particles: a review of observations, *J. Aerosol Sci.*, 35(2), 143–176, doi:10.1016/j.jaerosci.2003.10.003, 2004.
- Kulmala, M., Riipinen, I., Sipilä, M., Manninen, H. E., Petäjä, T., Junninen, H., Maso, M. D., Mordas, G., Mirme, A., Vana, M., Hirsikko, A., Laakso, L., Harrison, R. M., Hanson, I., Leung, C., Lehtinen, K. E. J.

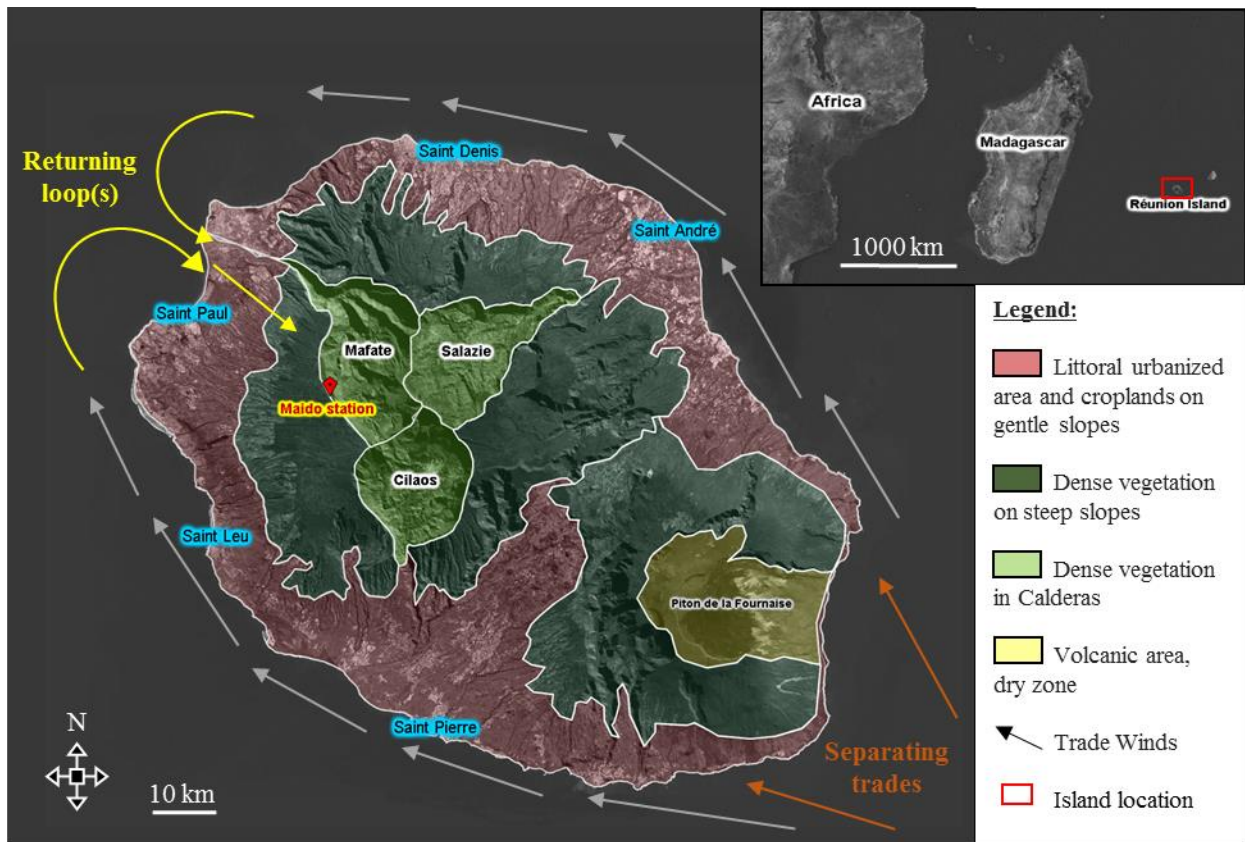
- and Kerminen, V.-M.: Toward Direct Measurement of Atmospheric Nucleation, *Science*, 318(5847), 89–92, doi:10.1126/science.1144124, 2007.
- 530 Lehtinen, K. E. J., Dal Maso, M., Kulmala, M. and Kerminen, V.-M.: Estimating nucleation rates from apparent particle formation rates and vice versa: Revised formulation of the Kerminen–Kulmala equation, *J. Aerosol Sci.*, 38(9), 988–994, doi:10.1016/j.jaerosci.2007.06.009, 2007.
- Lesouëf, D., Gheusi, F., Delmas, R. and Escobar, J.: Numerical simulations of local circulations and pollution transport over Reunion Island, *Ann. Geophys.*, 29(1), 53–69, doi:10.5194/angeo-29-53-2011, 2011.
- 535 Mäkelä, J. M., Riihelä, M., Ukkonen, A., Jokinen, V. and Keskinen, J.: Comparison of mobility equivalent diameter with Kelvin-Thomson diameter using ion mobility data, *J. Chem. Phys.*, 105(4), 1562–1571, doi:10.1063/1.472017, 1996.
- Makkonen, R., Asmi, A., Kerminen, V.-M., Boy, M., Arneth, A., Hari, P. and Kulmala, M.: Air pollution control and decreasing new particle formation lead to strong climate warming, *Atmospheric Chem. Phys.*, 12(3), 1515–1524, doi:10.5194/acp-12-1515-2012, 2012.
- 540 Manninen, H. E., Nieminen, T., Asmi, E., Gagné, S., Häkkinen, S., Lehtipalo, K., Aalto, P., Vana, M., Mirme, A., Mirme, S., Hörrak, U., Plass-Dülmer, C., Stange, G., Kiss, G., Hoffer, A., Törő, N., Moerman, M., Henzing, B., de Leeuw, G., Brinkenberg, M., Kouvarakis, G. N., Bougiatioti, A., Mihalopoulos, N., O’Dowd, C., Ceburnis, D., Arneth, A., Svenningsson, B., Swietlicki, E., Tarozzi, L., Decesari, S., Facchini, M. C., Birmili, W., Sonntag, A., Wiedensohler, A., Boulon, J., Sellegri, K., Laj, P., Gysel, M., Bukowiecki, N., Weingartner, E., Wehrle, G., Laaksonen, A., Hamed, A., Joutsensaari, J., Petäjä, T., Kerminen, V.-M. and Kulmala, M.: EUCAARI ion spectrometer measurements at 12 European sites – analysis of new particle formation events, *Atmos Chem Phys*, 10(16), 7907–7927, doi:10.5194/acp-10-7907-2010, 2010.
- 550 Martin, S. T., Andreae, M. O., Artaxo, P., Baumgardner, D., Chen, Q., Goldstein, A. H., Guenther, A., Heald, C. L., Mayol-Bracero, O. L., McMurry, P. H., Pauliquevis, T., Pöschl, U., Prather, K. A., Roberts, G. C., Saleska, S. R., Silva Dias, M. A., Spracklen, D. V., Swietlicki, E. and Trebs, I.: Sources and properties of Amazonian aerosol particles, *Rev. Geophys.*, 48(2), RG2002, doi:10.1029/2008RG000280, 2010.
- 555 Mikkonen, S., Lehtinen, K. E., Hamed, A., Joutsensaari, J., Facchini, M. C. and Laaksonen, A.: Using discriminant analysis as a nucleation event classification method, *Atmospheric Chem. Phys.*, 6(12), 5549–5557, 2006.
- Mikkonen, S., Romakkaniemi, S., Smith, J. N., Korhonen, H., Petäjä, T., Plass-Duelmer, C., Boy, M., McMurry, P. H., Lehtinen, K. E. J., Joutsensaari, J., Hamed, A., Mauldin III, R. L., Birmili, W., Spindler, G., Arnold, F., Kulmala, M. and Laaksonen, A.: A statistical proxy for sulphuric acid concentration, *Atmospheric Chem. Phys.*, 11(21), 11319–11334, doi:10.5194/acp-11-11319-2011, 2011.
- Mirme, A., Tamm, E., Mordas, G., Vana, M., Uin, J., Mirme, S., Bernotas, T., Laakso, L., Hirsikko, A. and Kulmala, M.: A wide-range multi-channel Air Ion Spectrometer, *Boreal Environ.*, 12, 247–264, 2007.
- 565 Modini, R. L., Ristovski, Z. D., Johnson, G. R., He, C., Surawski, N., Morawska, L., Suni, T. and Kulmala, M.: New particle formation and growth at a remote, sub-tropical coastal location, *Atmospheric Chem. Phys.*, 9(19), 7607–7621, 2009.
- Peltier, A., Beauducel, F., Villeneuve, N., Ferrazzini, V., Di Muro, A., Aiuppa, A., Derrien, A., Jourde, K. and Taisne, B.: Deep fluid transfer evidenced by surface deformation during the 2014–2015 unrest at

- 570 Piton de la Fournaise volcano, *J. Volcanol. Geotherm. Res.*, 321, 140–148, doi:10.1016/j.jvolgeores.2016.04.031, 2016.
- Petäjä, T., Mauldin Iii, R. L., Kosciuch, E., McGrath, J., Nieminen, T., Paasonen, P., Boy, M., Adamov, A., Kotiaho, T. and Kulmala, M.: Sulfuric acid and OH concentrations in a boreal forest site, *Atmospheric Chem. Phys.*, 9(19), 7435–7448, 2009.
- 575 Rose, C., Sellegri, K., Velarde, F., Moreno, I., Ramonet, M., Weinhold, K., Krejci, R., Ginot, P., Andrade, M., Wiedensohler, A. and Laj, P.: Frequent nucleation events at the high altitude station of Chacaltaya (5240 m a.s.l.), Bolivia, *Atmos. Environ.*, 102, 18–29, doi:10.1016/j.atmosenv.2014.11.015, 2015a.
- 580 Rose, C., Sellegri, K., Velarde, F., Moreno, I., Ramonet, M., Weinhold, K., Krejci, R., Ginot, P., Andrade, M., Wiedensohler, A. and Laj, P.: Frequent nucleation events at the high altitude station of Chacaltaya (5240 m a.s.l.), Bolivia, *Atmos. Environ.*, 102, 18–29, doi:10.1016/j.atmosenv.2014.11.015, 2015b.
- 585 Rose, C., Sellegri, K., Asmi, E., Hervo, M., Freney, E., Colomb, A., Junninen, H., Duplissy, J., Sipilä, M., Kontkanen, J., Lehtipalo, K. and Kulmala, M.: Major contribution of neutral clusters to new particle formation at the interface between the boundary layer and the free troposphere, *Atmos Chem Phys*, 15(6), 3413–3428, doi:10.5194/acp-15-3413-2015, 2015c.
- Seinfeld, J. H. and Pandis, S. N.: *Atmospheric Chemistry and Physics: From Air Pollution to Climate Change*, Third edition., John Wiley & Sons, New York., 2016.
- 590 Sihto, S.-L., Kulmala, M., Kerminen, V.-M., Maso, M. D., Petäjä, T., Riipinen, I., Korhonen, H., Arnold, F., Janson, R., Boy, M. and others: Atmospheric sulphuric acid and aerosol formation: implications from atmospheric measurements for nucleation and early growth mechanisms, *Atmospheric Chem. Phys.*, 6(12), 4079–4091, 2006.
- Soler, O.: *Atlas climatique de La Réunion (study report, 77p).*, 2000.
- 595 Tulet, P. and Villeneuve, N.: Large scale modeling of the transport, chemical transformation and mass budget of the sulfur emitted during the April 2007 eruption of Piton de la Fournaise, *Atmospheric Chem. Phys.*, 11(9), 4533–4546, doi:10.5194/acp-11-4533-2011, 2011.
- 600 Tulet, P., Di Muro, A., Colomb, A., Denjean, C., Duflot, V., Arellano, S., Foucart, B., Brioude, J., Sellegri, K., Peltier, A., Aiuppa, A., Barthe, C., Bhugwant, C., Bielli, S., Boissier, P., Boudoire, G., Bourrienne, T., Brunet, C., Burnet, F., Cammas, J.-P., Gabarrot, F., Galle, B., Giudice, G., Guadagno, C., Jeamblu, F., Kowalski, P., Leclair de Bellevue, J., Marquestaut, N., Mékies, D., Metzger, J.-M., Pianezze, J., Portafaix, T., Sciare, J., Tournigand, A. and Villeneuve, N.: First results of the Piton de la Fournaise STRAP 2015 experiment: multidisciplinary tracking of a volcanic gas and aerosol plume, *Atmospheric Chem. Phys.*, 17(8), 5355–5378, doi:10.5194/acp-17-5355-2017, 2017a.
- 605 Tulet, P., Di Muro, A., Colomb, A., Denjean, C., Duflot, V., Arellano, S., Foucart, B., Brioude, J., Sellegri, K., Peltier, A., Aiuppa, A., Barthe, C., Bhugwant, C., Bielli, S., Boissier, P., Boudoire, G., Bourrienne, T., Brunet, C., Burnet, F., Cammas, J.-P., Gabarrot, F., Galle, B., Giudice, G., Guadagno, C., Jeamblu, F., Kowalski, P., Leclair de Bellevue, J., Marquestaut, N., Mékies, D., Metzger, J.-M., Pianezze, J., Portafaix, T., Sciare, J., Tournigand, A. and Villeneuve, N.: First results of the Piton de la Fournaise STRAP 2015 experiment: multidisciplinary tracking of a volcanic gas and aerosol plume, *Atmos Chem Phys*, 17(8), 5355–5378, doi:10.5194/acp-17-5355-2017, 2017b.
- 610

- Vakkari, V., Laakso, H., Kulmala, M., Laaksonen, A., Mabaso, D., Molefe, M., Kgabi, N. and Laakso, L.: New particle formation events in semi-clean South African savannah, *Atmospheric Chem. Phys.*, 11(7), 3333–3346, doi:10.5194/acp-11-3333-2011, 2011.
- 615 Venzac, H., Sellegri, K., Laj, P., Villani, P., Bonasoni, P., Marinoni, A., Cristofanelli, P., Calzolari, F., Fuzzi, S., Decesari, S. and others: High frequency new particle formation in the Himalayas, *Proc. Natl. Acad. Sci.*, 105(41), 15666–15671, 2008.
- 620 Wiedensohler, A., Birmili, W., Nowak, A., Sonntag, A., Weinhold, K., Merkel, M., Wehner, B., Tuch, T., Pfeifer, S., Fiebig, M., Fjåraa, A. M., Asmi, E., Sellegri, K., Depuy, R., Venzac, H., Villani, P., Laj, P., Aalto, P., Ogren, J. A., Swietlicki, E., Williams, P., Roldin, P., Quincey, P., Hüglin, C., Fierz-Schmidhauser, R., Gysel, M., Weingartner, E., Riccobono, F., Santos, S., Grüning, C., Faloon, K., Beddows, D., Harrison, R., Monahan, C., Jennings, S. G., O’Dowd, C. D., Marinoni, A., Horn, H.-G., Keck, L., Jiang, J., Scheckman, J., McMurry, P. H., Deng, Z., Zhao, C. S., Moerman, M., Henzing, B., De Leeuw, G., Löschau, G. and Bastian, S.: Mobility particle size spectrometers: harmonization of technical standards and data structure to facilitate high quality long-term observations of atmospheric particle number size distributions, *Atmospheric Meas. Tech.*, 5, 657–685, doi:10.5194/amt-5-657-2012, 2012.
- 630 Yli-Juuti, T., Nieminen, T., Hirsikko, A., Aalto, P. P., Asmi, E., Hörrak, U., Manninen, H. E., Patokoski, J., Dal Maso, M., Petäjä, T., Rinne, J., Kulmala, M. and Riipinen, I.: Growth rates of nucleation mode particles in Hyytiälä during 2003–2009: variation with particle size, season, data analysis method and ambient conditions, *Atmospheric Chem. Phys.*, 11(24), 12865–12886, doi:10.5194/acp-11-12865-2011, 2011.
- Yu, F., Wang, Z., Luo, G. and Turco, R.: Ion-mediated nucleation as an important global source of tropospheric aerosols, *Atmospheric Chem. Phys.*, 8(9), 2537–2554, 2008.
- 635 Yu, F., Luo, G., Nadykto, A. B. and Herb, J.: Impact of temperature dependence on the possible contribution of organics to new particle formation in the atmosphere, *Atmos Chem Phys*, 17(8), 4997–5005, doi:10.5194/acp-17-4997-2017, 2017.

## Figures

Figure 1: Map of Reunion Island and its location. Different terrain types are represented as well as a simplification of the local atmospheric dynamic pattern around the island.



640

Figure 2: Dataset from 2015 Maïdo campaign. Devices recorded data simultaneously from May to November.

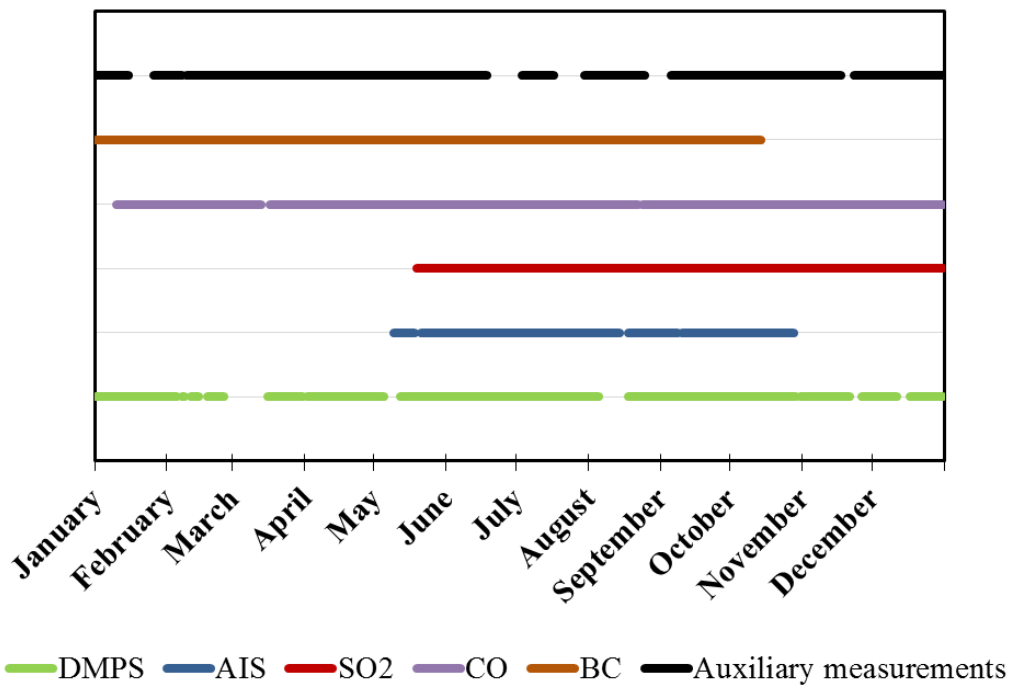
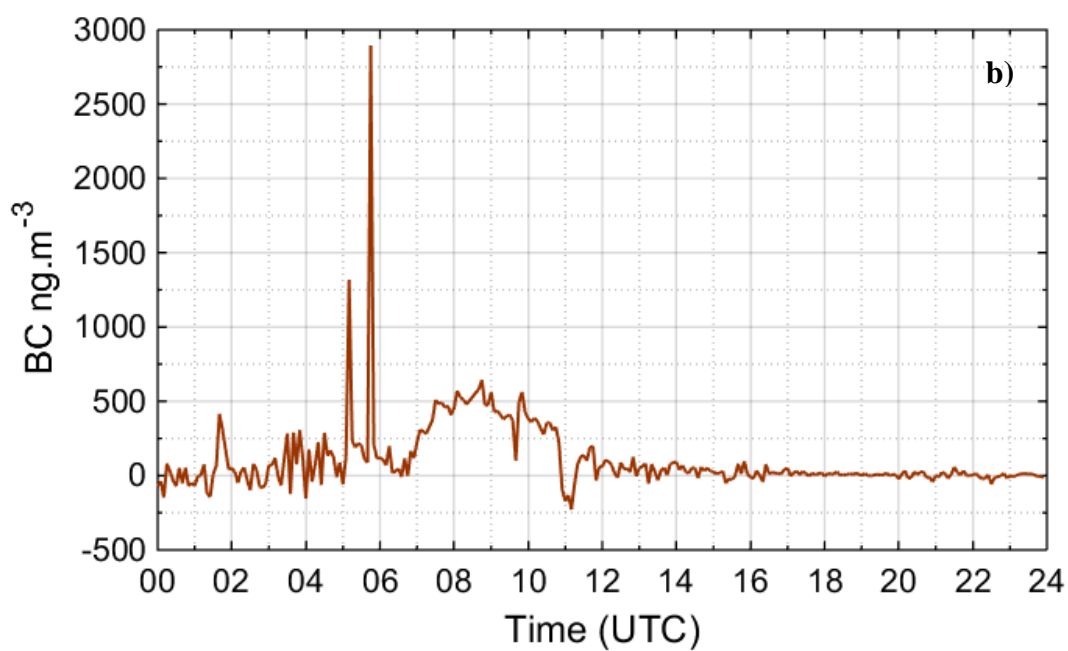
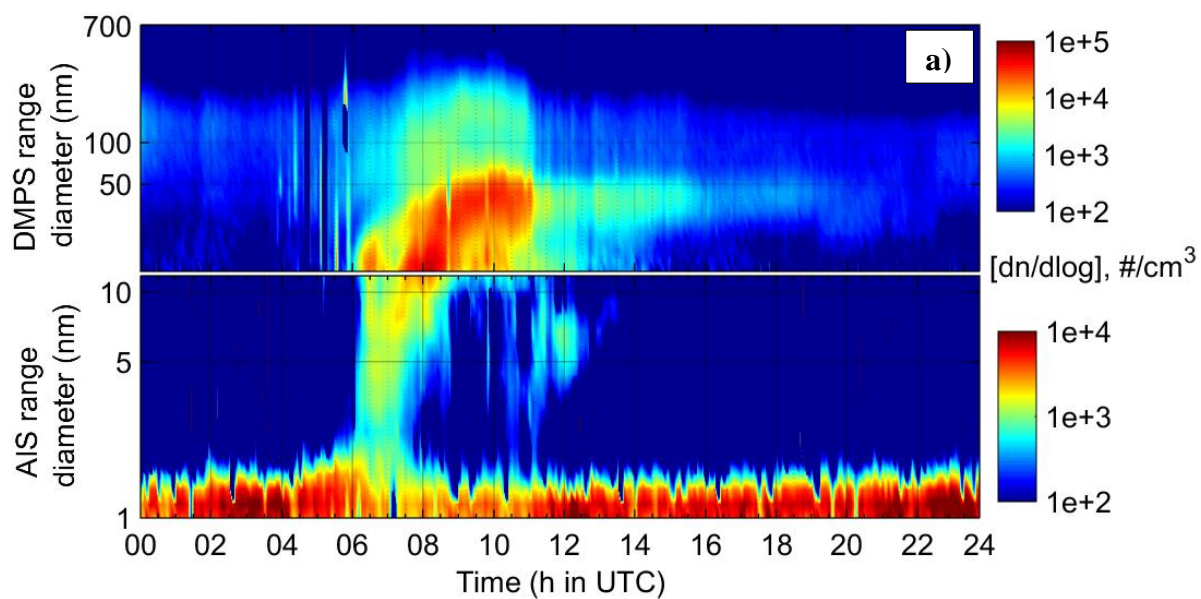
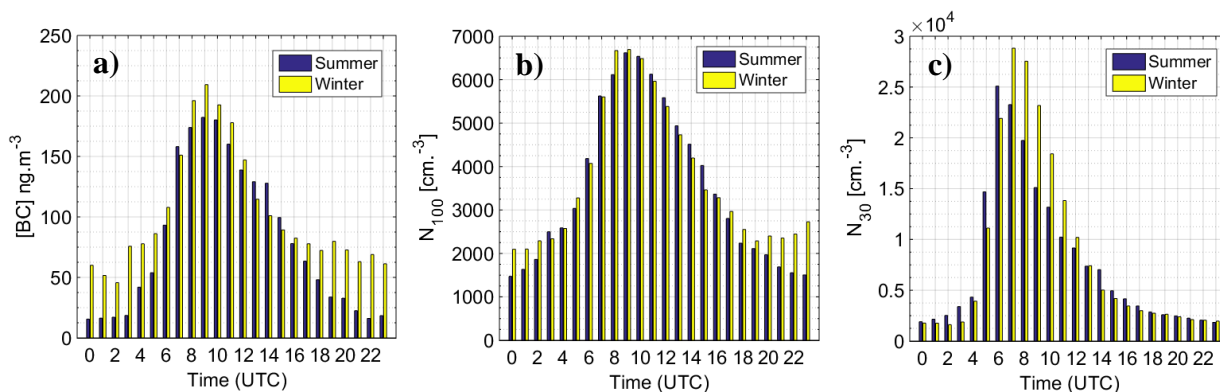


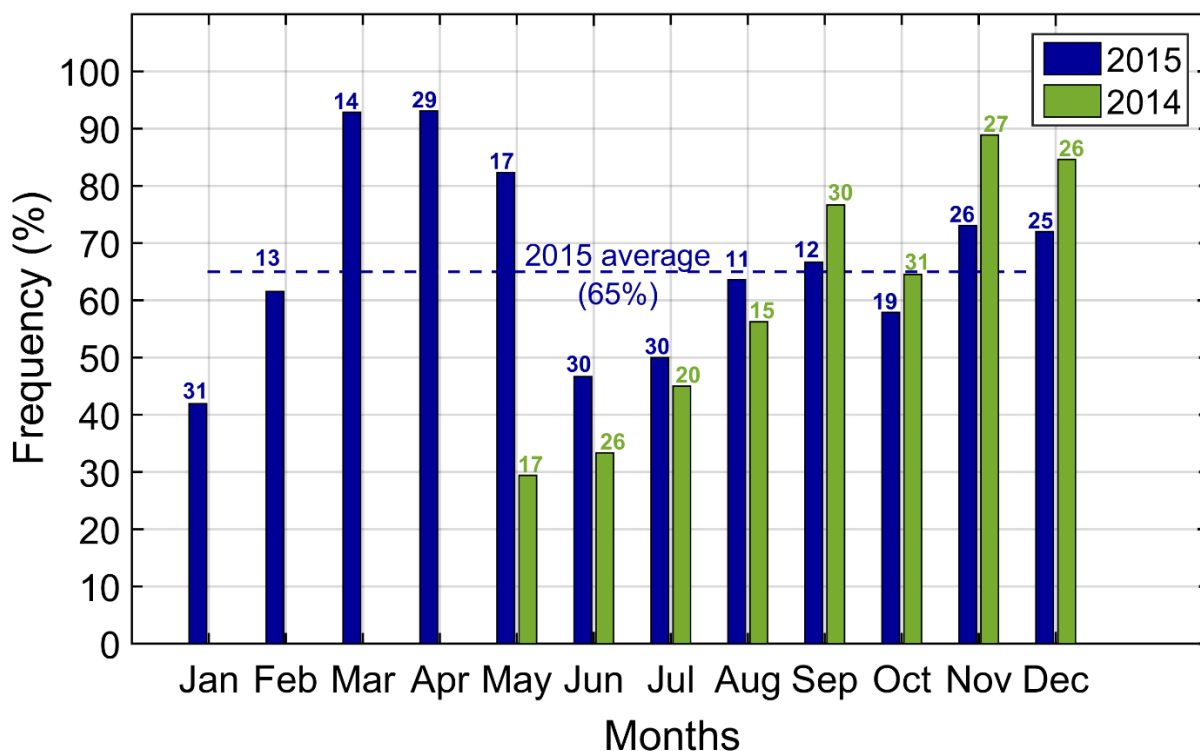
Figure 3: July 6<sup>th</sup> 2015 diurnal variation of (a) negative ions (1-10 nm) and (10-700 nm) aerosol particle size distribution (note the different concentration scales for ion number and particle concentrations), and (b) the BC concentration variation in  $\text{ng.m}^{-3}$



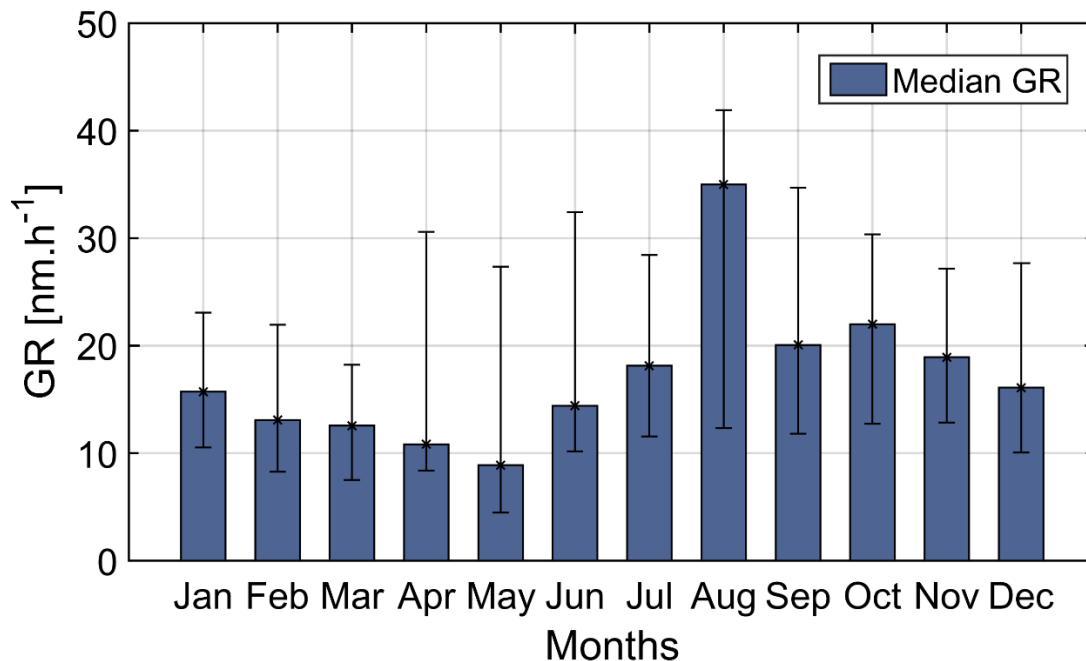
**Figure 4: Average diurnal variation during winter and summer of the (a) BC concentration, (b) number concentration of particles which diameter is larger than 100 nm ( $N_{100}$ ) and (c) number concentration of particles which diameter is smaller than 30 nm ( $N_{30}$ ).**



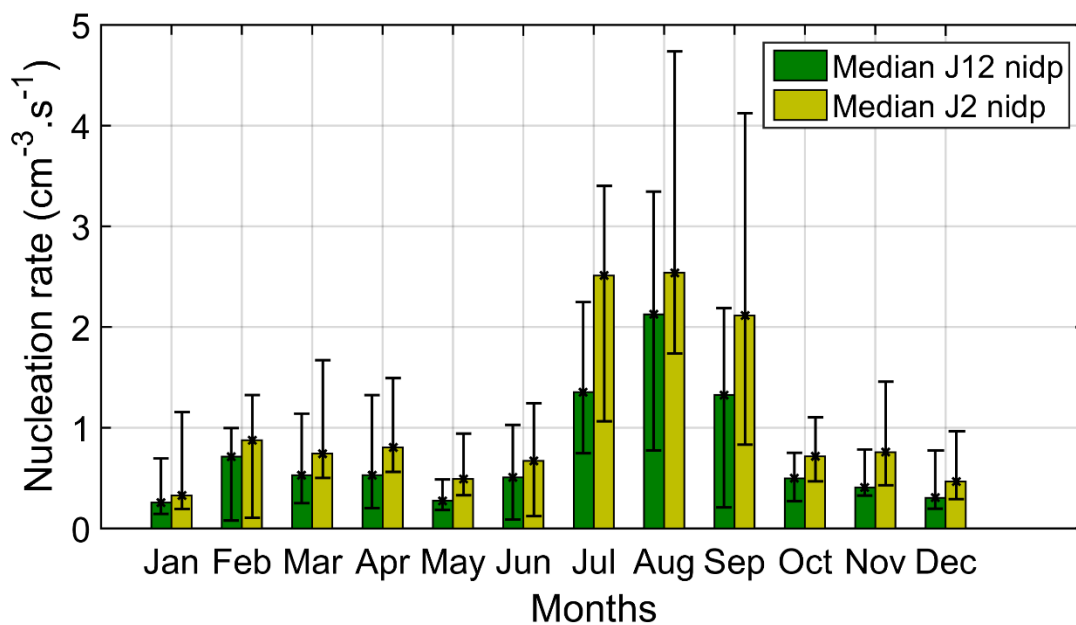
**Figure 5: Monthly event frequency (%) variation during 2014 (green) and 2015 (blue). Values at the top of the bars correspond to the number of days that were taken in account for calculation.**



655 **Figure 6: Monthly median growth rates in 2015. Error bars in black represent 25ile (top) and 75ile (base). To build these representation, 146 growth rates were estimated on 167 days classified as event days.**

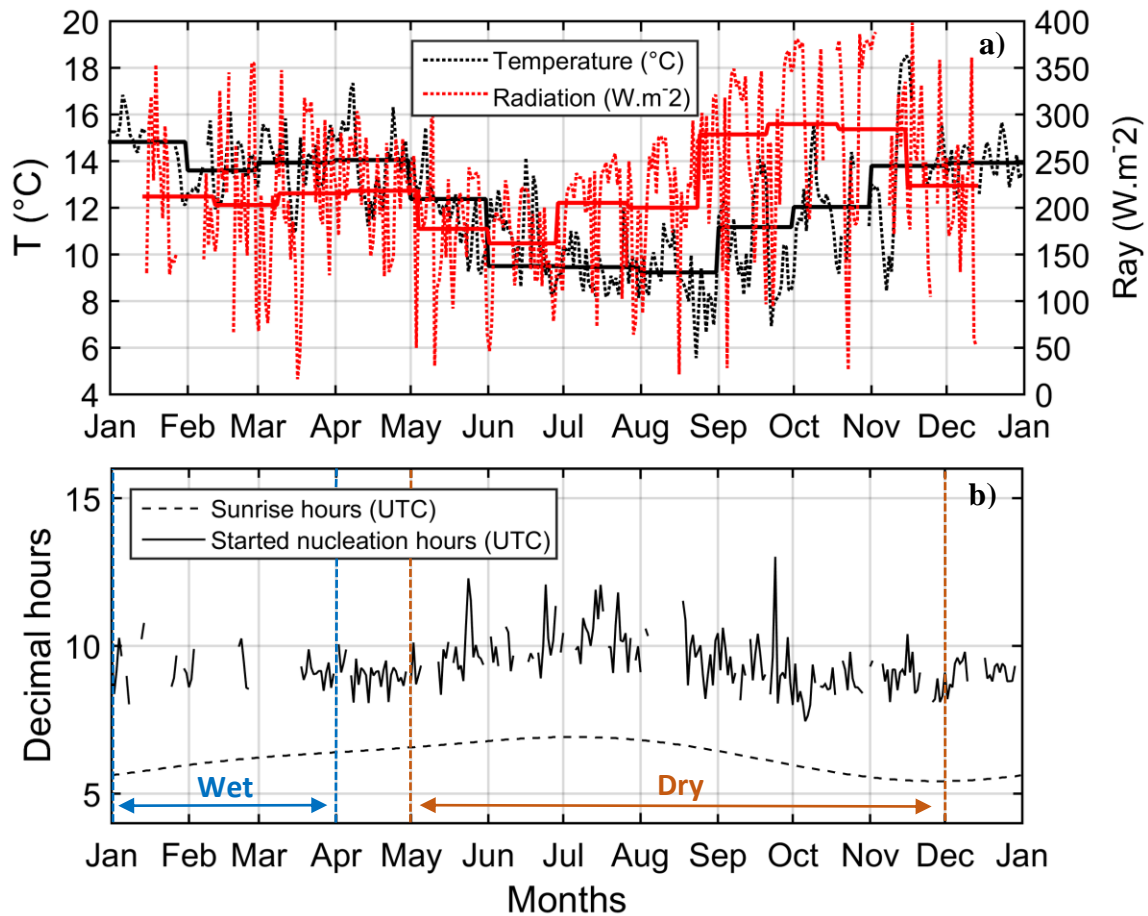


**Figure 7: Monthly median nucleation rates in 2015 for 2 and 12 nm sizes. Error bars in black represent 25ile (top) and 75ile (base).**

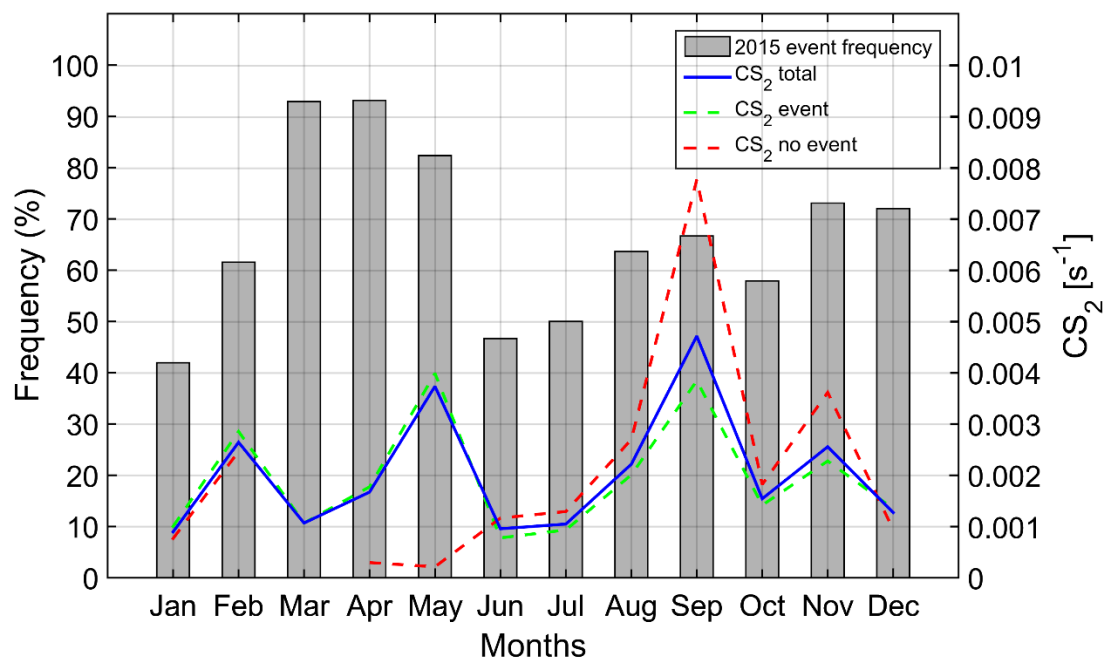


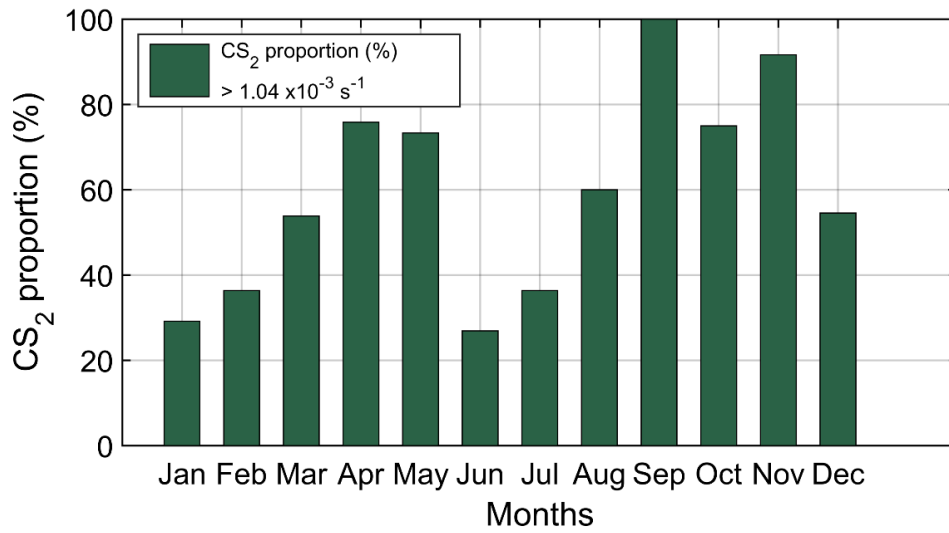
660

Figure 8: a) temperature ( $^{\circ}\text{C}$ ) and incidental radiation ( $\text{W}\cdot\text{m}^{-2}$ ) variations during 2015 at Maido station given by daily UTC (fine) and monthly (bold) averages; b) seasonal variation of sunrise and time of NPF onset in UTC. The dry and the wet seasons are also delimited in orange and blue respectively.



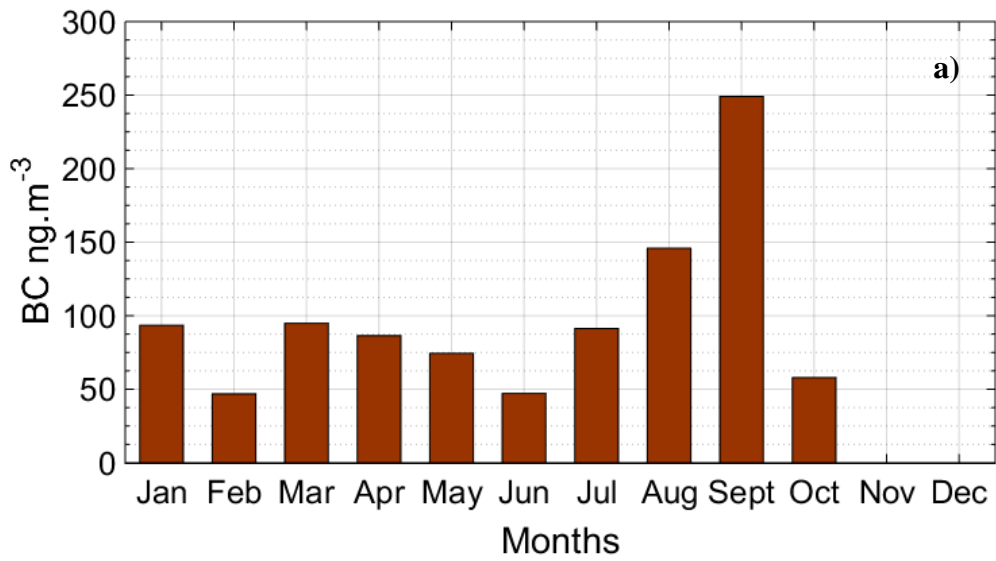
665 Figure 9: (a) Monthly  $\text{CS}_2$  (blue) calculated two hours before NPF onset (scale at the right in  $\text{s}^{-1}$ ) and monthly event frequency  $f_m$  (scale at the left in percentage). Averages have been calculated for event days (green), non-event days (red) and all days (blue). (b) Monthly  $\text{CS}_2$  proportion exceeding the average of  $\text{CS}_{2\text{ev}}$  and  $\text{CS}_{2\text{noev}}$  medians ( $1.04 \times 10^{-3} \text{ s}^{-1}$ ).

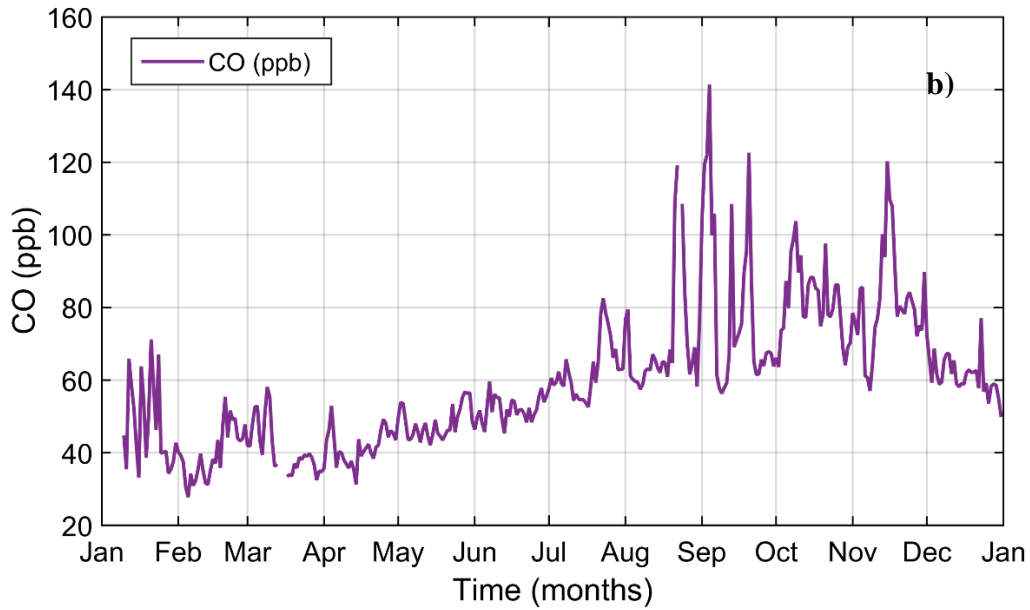




670

Figure 10: Monthly averages of the (a) BC concentration (ng.m-3) and (b) CO concentration (ppb) during the year 2015





675 Table 1: Annual statistical values for  $G_{12-19}$ ;  $J_{12}$ ;  $J_2$ ; CS and  $CS_2$  calculated on daily averages.

	$GR_{12-19}$ (nm.h <sup>-1</sup> )	$J_{12}$ (cm <sup>-3</sup> .s <sup>-1</sup> )	$J_2$ (cm <sup>-3</sup> .s <sup>-1</sup> )	CS (s <sup>-1</sup> )	$CS_2$ (s <sup>-1</sup> )
<b>Averages</b>	<b>19.455</b>	<b>0.931</b>	<b>1.531</b>	<b><math>2.43 \times 10^{-3}</math></b>	<b><math>1.86 \times 10^{-3}</math></b>
Standard dev.	12.689	1.153	0.920	$2.06 \times 10^{-3}$	$2.53 \times 10^{-3}$
<b>Medians</b>	<b>15.16</b>	<b>0.508</b>	<b>0.858</b>	<b><math>1.97 \times 10^{-3}</math></b>	<b><math>1.15 \times 10^{-3}</math></b>
25ile	9.58	0.223	0.385	$1.19 \times 10^{-3}$	$6.55 \times 10^{-4}$
75ile	27.69	1.131	1.756	$2.96 \times 10^{-3}$	$2.00 \times 10^{-3}$

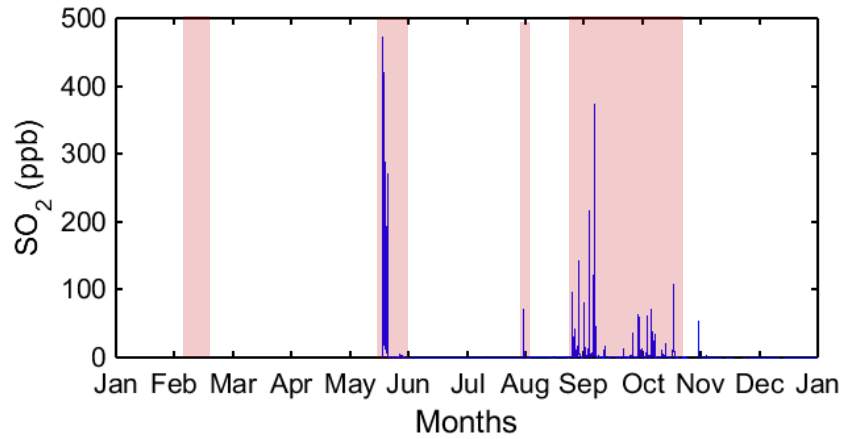
**Table 2: R correlation coefficients giving the relationships between NPF parameters (occurrence, GR and Js) and influencing factors (Ray, RH, T, P,  $CS_2$ ,  $CS_{2prop}$ , CO and BC).**

R	NPF %	$GR_{12-19}$	$J_{12}$	$J_2$
Ray	0,096	0,284	0,012	0,062
RH	0,056	0,406	0,528	<b>0,689</b>
T	0,411	0,536	<b>0,717</b>	<b>0,732</b>
P	0,051	0,426	0,524	<b>0,597</b>
$CS_2$	0,217	0,020	0,179	0,167
$CS_{2prop}$	0,546	0,152	0,079	0,124
CO	0,234	<b>0,638</b>	0,326	0,389
BC	0,103	0,418	<b>0,576</b>	<b>0,601</b>

680 Correlations have been calculated with the twelve 2015 monthly averages for each parameters. Taking a degrees-of-freedom value of 10 and a risk  $\alpha = 0.05$  (95% of confidence), we obtained a lower limit value of 0.576 according to the Pearson table. The highlighted R in the table are above the limit value meaning that the variables are significantly dependent.

## Appendices

685 **Figure A1: SO<sub>2</sub> concentration (ppb) at Maïdo station in 2015, showing the occurrence of three eruptive periods in red (17 to 30/05, 31/07 to 02/08 and 24/08 to 18/10)**



690 Sulfur dioxide concentrations allow us to distinguish days when NPF can be affected by the presence of the volcanic plume. Based on a 1 ppb threshold, which was the 97th percentile of the series, we considered that 47 days were plume days at the Maïdo station and removed them. The eruptive periods are clearly visible on this figure.

**Table A1: Meteorological parameter averages.**

	<b>Ray (W.m<sup>-2</sup>)</b>	<b>RH (%)</b>	<b>T (°C)</b>	<b>P (hPa)</b>
January	212.07	78.77	14.82	787.21
February	202.98	77.17	13.60	788.85
March	215.42	74.11	13.93	789.45
April	218.26	66.70	14.05	789.41
May	177.43	72.20	12.38	791.51
June	161.91	70.00	9.50	790.90
July	205.30	53.78	9.46	792.52
August	200.18	64.46	9.23	791.93
September	278.64	50.02	11.17	791.02
October	289.73	63.55	12.04	791.92
November	248.20	56.26	13.80	789.91
December	223.63	77.10	13.92	790.16
<b>Yearly average</b>	<b>222.48</b>	<b>67.01</b>	<b>12.32</b>	<b>790.40</b>

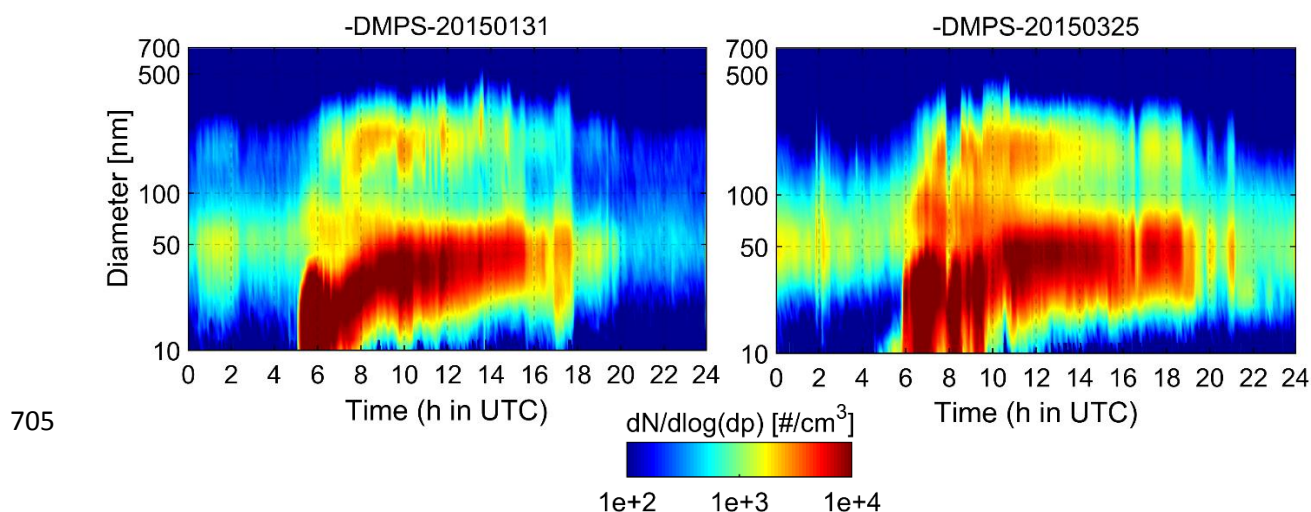
695 **Table A2: Comparison of NPF frequency, GR, J and CS values**

<i>Study</i>	<i>Location</i>	<i>Environment</i>	<i>NPF (%)</i>	<i>GR (nm.h<sup>-1</sup>)</i>	<i>J (cm<sup>3</sup>.s<sup>-1</sup>)</i>	<i>CS (s<sup>-1</sup>)</i>
<i>Dal Maso (2002)</i>	Ireland	Coastal	-	15 to 180	300 to 10000	$2 \times 10^{-3}$
<i>Koponen (2003)</i>	Antarctica	Coastal	-	1 - 2	0.5	-
<i>Iida (2008)</i>	Mexico	Urban	-	18	1900 to 3000	-
<i>McMurry (2003)</i>	Atlanta, GA	Urban	-	2 – 6	20 to 70	-
<i>Venzac (2008)</i>	Nepal	Altitude	35%	2	< 0.2	$2.1 \times 10^{-3}$
<i>Modini (2009)</i>	Australia	Coastal	65%	19	-	
<i>Vakkari (2011)</i>	South Africa	Remote, Altitude, Savannah	69%	2.1 to 30	0.1 to 28	$4.3 \times 10^{-3}$
<i>Boulon (2011)</i>	France	Altitude	35.9%	6.20	1.382	$3.7 \times 10^{-3}$
<i>Hirsikko (2012)</i>	South Africa	Remote, Altitude, Savannah	86%	$8.0 \pm 4.1$	$4.5 \pm 6.1$	$0.8 \times 10^{-2}$
<i>Rose (2015)</i>	Bolivia	Altitude	63.9%	7.62	-	$2.4 \times 10^{-3}$
<b><i>Our study</i></b>	<b>Reunion</b>	<b>Coastal, Altitude</b>	<b>65%</b>	<b>GR<sub>12-19</sub> = 19.455</b>	<b>J<sub>12</sub> = 0.931, J<sub>2</sub> = 1.531</b>	<b><math>2.43 \times 10^{-3}</math></b>

This table is given to help in the comparison of NPF parameters as a function of the different types of environments. A few stations are listed here. The values of the present study are summarized in the last line and the closest ones are highlighted (yellow). Reunion Island seems to present NPF characteristics of several environment types. The GRs and Js listed in the table are in a similar range to those estimated in the present study.

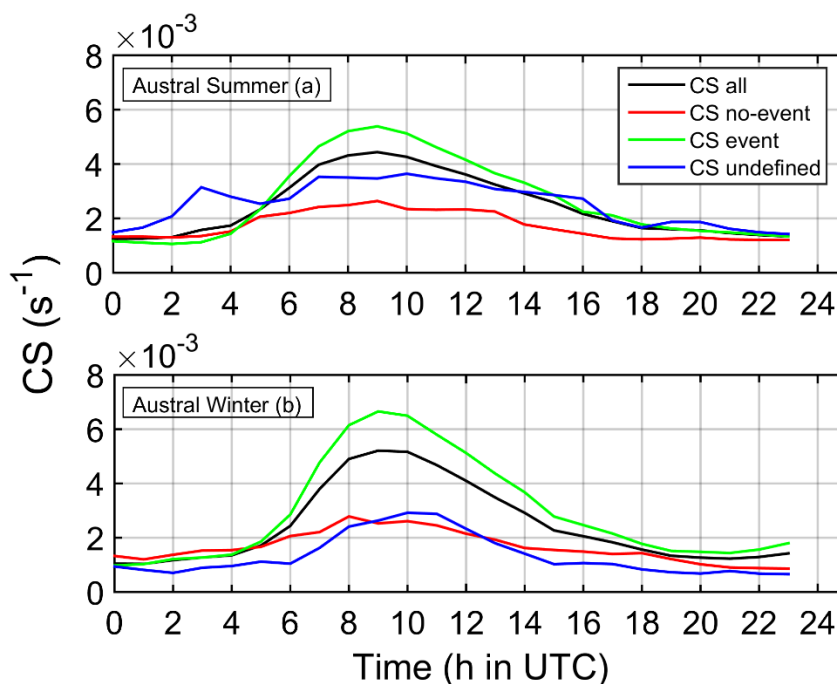
700

Figure A2: DMPS spectra for 31 January on the left and 25 March on the right. This is an evolution of the size distribution (left scale in nanometres) and of the aerosol concentration (colorimetric scale) with time (from 00 to 24 UTC).



705

Figure A3: Diurnal variation of CS



710

As the CS parameter varies throughout the day, we have also chosen to show the average daily variation of CS for summer a) and for winter b). Averages were calculated on undefined ( $CS_{un}$ ), no-event ( $CS_{noev}$ ), event ( $CS_{ev}$ ) and all days. Maximum of CS all and  $CS_{ev}$  are reached at 9:00 UTC for both seasons but are higher for winter ( $CS_{all} = 5.1 \times 10^{-3} \text{ s}^{-1}$ ;  $CS_{ev} = 6.9 \times 10^{-3} \text{ s}^{-1}$ ) than summer ( $CS_{all} = 4.5 \times 10^{-3} \text{ s}^{-1}$ ;  $CS_{ev} = 5.2 \times 10^{-3} \text{ s}^{-1}$ ).  $CS_{ev}$  really begins to increase at 4:00 UTC for summer but 5:00 UTC for winter. This corresponds to the moment when  $CS_{noev}$  becomes lower than  $CS_{ev}$ . Before these times,  $CS_{noev}$  is  $10^{-4}$  higher than  $CS_{ev}$ , implying that  $CS_{noev}$  is too large to trigger new

715 particle formation. Consequently, and thanks to this daily representation, we assume that CS affects the new  
particle formation trigger for both seasons in 2015. Moreover, it can be seen that  $CS_{un}$  curves follow the  $CS_{noev}$   
720 curves better than  $CS_{ev}$  so it is possible that no-event days were not well recognized.

**Figure A4: DMPS spectra for a) April and b) June months. We can clearly observe an event number difference between the two months according to the different FNP occurrence averages which are 93.1% for April and 46.7% for June.**

